UNIVERSITY OF CALIFORNIA SAN DIEGO

Synthetic Lethal Interaction Between BRCA1 and FEN1 in Ovarian Cancer Cells

A Thesis submitted in partial satisfaction of the
requirements for the degree Master of Science

in

Biology

by

Yueyang Huang

Committee in charge:

Professor Jean Y.J. Wang, Chair
Professor Nan Hao, Co-Chair
Professor Lorraine Pillus

2021

The Thesis of Yueyang Huang is approved, and it is acceptable in quality and form for publication on microfilm and electronically.

University of California San Diego

2021

TABLE OF CONTENTS

LIST OF ABBREVIATIONS

Abbreviations	Definitions
BACH1	BRCA1-associated carboxyl-terminal helicase
BARD1	BRCA1-associated ring domain 1
BPE	bovine pituitary extract
BRCA1	breast cancer type 1 susceptibility gene
BRCT	BRCA1-associated C-terminal
CBA	chicken-ß-actin
CHK1	checkpoint kinase 1
CRISPR	clustered regularly interspaced short palindromic repeats
crRNA	CRISPR RNA
CtIP	CtBP-interacting protein
DMEM	Dulbecco's Modified Eagle's Medium
DSB	double-stranded break
EDTA	ethylenediaminetetraacetate
FACS	fluorescence-activated cell sorting
FBS	fetal bovine serum
FEN1/RAD27	flap endonuclease 1
GEN	gap-endonuclease
GH	growth hormone
HC	hydrocortisone
hCG	human chorionic gonadotropin
HDR	homology-directed repair
hEGF	human epidermal growth factor
HR	homologous recombination
LP-BER	long-patch base excision repair
MEBM	Mammary Epithelial Cell Basal Medium
NHEJ	non-homologous end joining
NLS	nuclear localization signal
OSE	ovarian surface epithelial
PALB2	partner and localizer of BRCA2
PARP	poly-ADP-ribosyl polymerase
PBS	phosphate-buffered saline
RPMI	Roswell Park Memorial Institute
SGA	synthetic genetic arrays
sgRNA	single-guide RNA
SL	synthetic lethality
SSB	single-stranded break
tracRNA	trans-activating crRNA

LIST OF FIGURES

LIST OF TABLES

ACKNOWLEDGMENTS

I would like to express my deepest appreciation to my advisor, Professor Jean Wang, for guiding and supporting me throughout my MS study. She provided me with invaluable feedback and advice in all the time of research and writing of this thesis. My completion of the MS would not have been possible without her patience and continuous help.

Besides my advisor, I would like to thank my committee members: Professor Nan Hao and Professor Lorraine Pillus, for their guidance through this process.

I am also grateful to Dr. Richard Kolodner for offering me the opportunity to work as a lab assistant in his group which helped fund my education and allowed me to participate in diverse exciting projects.

I would like to extend my sincere thanks to the research scientists and my labmates in the group for the constant assistance and encouragement.

Last but not least, I would like to thank my parents and friends for always being there, supporting me and cheering me up when I am down. I undoubtedly could not have gone this far without them.

ABSTRACT OF THE THESIS

Synthetic Lethal Interaction Between BRCA1 and FEN1 in Ovarian Cancer Cells

by

Yueyang Huang

Master of Science in Biology

University of California San Diego, 2021

Professor Jean Y.J. Wang, Chair
Professor Nan Hao, Co-Chair

The concept of synthetic lethality (SL) can be applied to selectively kill cancer cells by targeting SL-partners of a cancer-specific mutation. The SL-interaction between homologous recombination (HR) and the flap endonuclease was first established in yeast, and recently confirmed in human cells by showing that HR-deficient (*BRCA1*-deficient) cell lines are more sensitive to flap endonuclease 1 (FEN1)-inhibitors than *BRCA1*-proficient cell lines. To further establish that *BRCA1*-loss is sufficient to cause FEN1-inhibitor sensitivity in ovarian cancer, I

used the CRISPR/Cas9 gene-editing methods to correct the *BRCA1* mutation in the FEN1-inhibitor sensitive UWB1.289 cells, and to knockout *BRCA1* in the FEN1-inhibitor resistant OV90 cells, followed by measuring the response of *BRCA1*-edited clones to FEN1-inhibitor SMD2485. With UWB1.289, I was unable to propagate plasmid-transfected cells, suggesting a possible sensitivity to exogenous DNA. With OV90, I found that the majority of edited *BRCA1*-alleles produced proteins with small in-frame deletions (ΔBRCA1) and that the few null-alleles underwent further mutations to produce ΔBRCA1 upon propagation in culture. I also found that ΔBRCA1-expressing clones were as resistant as the parental OV90 cells to SMD2485. Due to the sensitivity of UWB1.289 cells to transfection and the instability of *BRCA1*-null alleles in OV90 cells, this study failed to establish the sufficiency of *BRCA1*-loss in causing FEN1-inhibitor sensitivity. Alternative strategies to express *BRCA1*-wt in UWB1.289 cells and to overcome the instability of the *BRCA1*-null alleles in OV90 cells are discussed as future approaches to test the direct causal relationship between BRCA1-loss and FEN1-dependency in ovarian cancer.

CHAPTER 1 INTRODUCTION

1.1 Exploring Synthetic Lethal Genetic Interactions for Targeted Cancer Therapy

Synthetic lethality describes a negative genetic interaction that arises when combined defects in two or more genes lead to cell death, while a defect in each of these genes alone does not affect cell survival (Kaelin, 2005). 18.7% of the 5916 genes in yeast (96% of all known genes) when deleted individually were found to be required for cell survival and proliferation in rich medium (Giaever et al., 2002). The fact that more than 80% of yeast genes are not essential suggests that genes from the same or another functionally related biochemical pathway can compensate for the individual loss of those non-essential genes (Hartman IV et al., 2001; Tong et al., 2001). To uncover the functional relationships between genes on a large scale in yeast, Tong et.al (2001) developed synthetic genetic arrays (SGAs) to systematically generate double mutants by crossing a strain containing a query mutation with an array of ~4700 mutants, each having a nonessential deletion. Inviable double-mutant progenies imply that the two genes under investigation show a synthetic lethal interaction with each other (Tong et al., 2001). The SGAs can also be extended to elucidate genetic interactions among multiple genes by beginning with a query strain with more than one mutation (Tong et al., 2001). Such genetic screens have revealed a comprehensive genetic interaction network in yeast and have shown that synthetic lethal interactions are common among yeast genes (Tong et al., 2004).

Through a cross-species approach, van Pel and his research group (2013) found that 73% of the synthetic lethal interactions among chromosome instability genes identified in yeast were recapitulated in humans, suggesting that the knowledge of synthetic lethality can be extended beyond model organisms like yeast and be exploited in clinical and translational cancer research (Kaelin, 2005; Zhan & Lord, 2016). The idea of applying the synthetic lethal principle to cancer

treatment based on the results of yeast genetic screens was first proposed by Hartwell et.al (1997) and then Kaelin (2005) about 20 years ago and has become a widely accepted approach for anti-cancer drug development in recent years (Huang et al., 2020; Zhan & Lord, 2016). In principle, inhibitors of a non-essential gene showing synthetic lethal interaction with a tumor suppressor gene that is lost in tumor cells have the potential to selectively kill the tumor cells while sparing normal cells (Hartwell et al., 1997; Huang et al., 2020; Kaelin, 2005;). Many of the anticancer drugs used in clinics today are toxic to normal cells, which compromises the efficacy of these drugs in improving survival (Kaelin, 2005). Therefore, the concept of synthetic lethality offers great opportunities for the development of targeted cancer therapy, with the identification of tumor-specific synthetic lethal interactions as the crucial first step (Huang et al., 2020).

1.2 FEN1 Nuclease and Its Synthetic Lethal Partners Deduced from Yeast Genetics

Human flap endonuclease 1 (FEN1) with its 5'-flap endonuclease, 5'-exonuclease and gap-endonuclease (GEN) activities participates in various DNA metabolic processes including DNA replication and repair (Balakrishnan & Bambara, 2013; Zheng et al., 2011). In DNA replication, FEN1 binds and cuts at the base of single-stranded flap structure in Okazaki fragments, removing the RNA primer as well as the initial portion of the newly synthesized DNA and leaving a nick for ligation in the maturation of the lagging DNA strand (Balakrishnan & Bambara, 2013). In long-patch base excision repair (LP-BER), FEN1 binds and removes the 5'-flap generated as the result of strand-displacement synthesis by DNA polymerase β (Asagoshi et al., 2010; Balakrishnan & Bambara, 2013; Zheng et al., 2011). In resolution of stalled replication forks, the GEN activity of FEN1 has been identified to bind to ssDNA regions and cleave at the

ssDNA-dsDNA junctions of the stalled replication forks, leading to DSBs and subsequent break-induced recombination (Zheng et al., 2005; Zheng et al., 2011).

The functions and the synthetic lethal partners of the budding yeast *RAD27*, which is an evolutionarily conserved ortholog of *FEN1*, have been extensively studied in the yeast model genetic organism (Greene et al., 1999). In yeast, *RAD27* is not essential for cell survival likely because its role in processing Okazaki fragments can be carried out by other nucleases, such as Dna2 and Exo1, as well as the homologous recombination pathway that repairs stalled replication forks (Debrauwere et al., 2001). Nevertheless, mutants with *RAD27* deletion (*rad27Δ*) have higher mutation and recombination rates, are defective in long-patch base excision repair, and show sensitivity to temperature and UV radiation (Debrauwere et al., 2001; Tishkoff et al., 1997). Many synthetic lethal interactions have been identified between *RAD27* and other genes involved in DNA replication and repair, such as DNA helicase, *DNA2-1*, the DSB-repair genes (*RAD50-RAD59*) and 5'-exonuclease, *EXO 1* (Greene et al., 1999; Tishkoff et al., 1997). Deletions in any of the genes involved in homologous recombination (HR), including *RAD50*, *RAD51*, *RAD52*, *RAD54*, *RAD55*, *RAD57*, *MRE11 (RAD58)*, or *XRS2*, are not lethal but impair the ability of yeast to repair DSB by HR (Debrauwere et al., 2001). The fact that mutants with loss in both *RAD27* and HR genes are not viable demonstrates a synthetic lethal interaction between *RAD27* and HR genes and indicates that HR becomes an essential function in *RAD27*-defective cells (Debrauwere et al., 2001).

The highly conserved synthetic lethal interactions between yeast and human cells demonstrated by van Pel and his colleagues (2013) have led to the investigation of the evolutionary conservation of the RAD27-HR synthetic lethal interaction in humans. It has been shown that cells disrupted for MRE11A, the component of MRN (MRE11-RAD50-NBS1)

complex required for DSB recognition, are more sensitive to FEN1 inhibitors (van Pel et al., 2013; Ward et al., 2017). McManus et.al (2009) have also demonstrated that the SL interaction between the yeast *RAD54* and *RAD27* is conserved in humans between the highly sequence- and functionally similar *RAD54B* and *FEN1* genes. In addition to those core HR proteins that are conserved between yeast and humans, such as RAD54 and MRE11, FEN1 inhibition has been observed to sensitize cells disrupted for BRCA2, a protein not present in yeast but required for HR in humans and assumes the role of yeast RAD52 (Kowalczykowski, 2015; Ward et al., 2017). The results of these studies suggest that similar to its ortholog RAD27, FEN1 can be SL with many HR proteins in humans that are either conserved or non-conserved with yeast HR proteins. It also demonstrates the validity of deducing FEN1 SL partners in humans from yeast genetic studies.

1.3 BRCA1 Adaptor Protein and Its Role as a Suppressor of Ovarian Cancer

While the core HR mechanism is conserved from yeast to human, there exist human HR-genes that are not found in yeast but essential for homologous recombination repair in human cells, such as the protein encoded by the breast cancer type 1 susceptibility gene (BRCA1) (Hall et al., 1990; Kowalczykowski, 2015). Human *BRCA1*, mapped to chromosome 17q21, was discovered by genetic linkage studies as a gene underlying the inherited susceptibility to early-onset familial breast cancer as well as familial site-specific ovarian cancer (Hall et al., 1990; Steichen-Gersdorf et al., 1994). Miki et al. (1994) first cloned the *BRCA1* gene in 1994 and found it to encode a protein of 1863 amino acids. The BRCA1 protein contains a RING domain at the N-terminus and two tandem BRCA1-associated C-terminal (BRCT) domains at the C-terminus (Figure 1.1). The BRCA1 RING domain interacts with BRCA1-associated ring domain

1 (BARD1) protein, forming a heterodimer that has E3 ubiquitin ligase activity (Rosen, 2013; Takaoka & Miki, 2018). The BRCT domains bind to proteins containing phosphoserine or phosphotyrosine-motifs, including Abraxas, CtBP-interacting protein (CtIP) and BRCA1-associated carboxyl-terminal helicase (BACH1), and together they form complexes that are involved in DNA damage response and repair (Rosen, 2013; Takaoka & Miki, 2018). The coiled-coil domain is responsible for the association of BRCA1 with BRCA2 through the partner and localizer of BRCA2 (PALB2) protein (Takaoka & Miki, 2018).

Human BRCA1 is a multifunctional protein that plays a critical role in cellular responses to double-stranded DNA breaks (DSBs), including homologous recombination (HR)-dependent repair of DSBs, cell cycle checkpoint activation, transcriptional regulation, chromatin remodeling and apoptosis (Gudmundsdottir & Ashworth, 2006; Rosen, 2013; Takaoka & Miki, 2018; Paul, A. & Paul, S., 2014). In the initiation of HR, the BRCA1-CtIP complex interacts with the MRN (MRE11-RAD50-NBS1) complex to facilitate the resection of DSB ends by the nuclease activities of MRE11, producing 3' single-stranded DNA tail necessary for homology-dependent DNA strand invasion (Liu & Huang, 2016; Rosen, 2013; Sartori et al., 2007; Takaoka & Miki, 2018). In the execution of HR, through interaction with PALB2 (the partner and localizer of BRCA2), BRCA1 joins the PALB2-BRCA2-RAD51 complex to position the recombinase RAD51 at the resected single-stranded ends of DSBs (Rosen, 2013; Sy et al., 2009; Takaoka & Miki, 2018;). Thus, BRCA1 and BRCA2 are required for the formation of RAD51-coated ssDNA and the subsequent DNA homology search, ssDNA strand invasion, Holiday junction formation and the downstream repair synthesis (Godin et al., 2016). As a cell-cycle checkpoint regulator, the BRCA1-CtIP complex participates in the activation of checkpoint kinase 1 (CHK1) to enforce DSB-induced G2/M arrest that ensures the completion of DNA

replication prior to the onset of mitosis (Yu & Chen, 2004). The BRCA1-BACH1 complex can activate the intra-S checkpoint pathway, which is activated by DSB to cause a transient blockade of replication-initiation at replicons that have not yet fired in S-phase cells (Gong et al., 2010; Rosen, 2013; Takaoka & Miki, 2018). In addition to its function in HR and cell cycle checkpoints, BRCA1-BARD1 complex assists in resolving the R-loops that accumulate due to stalled RNA polymerase II during transcription, preventing R-loops from impeding DNA replication and leading to replication fork collapse (Tarsounas & Sung, 2020).

The functional studies of BRCA1 have demonstrated its crucial role in maintaining genome stability by activating DNA repair processes and cell cycle checkpoints and thus providing an understanding for how the loss of BRCA1 pre-disposes to the development of cancers (Paul, A. & Paul, S., 2014). Association studies have shown that carriers of *BRCA1* mutations are 20 times more likely to develop ovarian cancer and 7 times more likely to have breast cancer than individuals with wild-type *BRCA1* gene (Tarsounas & Sung, 2020). Almost all *BRCA1*-mutation carriers that develop cancers have tumors that lose the wild-type *BRCA1* allele and therefore have no functional BRCA1 (Rosen, 2013). The *BRCA1*-defective cells with impaired HR have to rely on non-homologous end joining (NHEJ), an alternative and error-prone DSB repair pathway that often introduces mutations and gives rise to genome instability, to repair DSBs (Rosen, 2013; Tarsounas & Sung, 2020). Furthermore, *BRCA1*-defective tumor cells are more likely to replicate and then propagate the mis-repaired DNA due to checkpoint deficiencies. These failures to respond to and to accurately repair DSBs jeopardizes genome integrity and fosters tumorigenesis (Tarsounas & Sung, 2020).

The role of BRCA1 as a tumor suppressor offers new opportunities to targeted cancer therapy for *BRCA1*-mutant cancer patients if genes that are synthetic lethal to *BRCA1* can be

identified. Previous research has discovered that *BRCA1/2*-deficient cancer cells are more sensitive to poly-ADP-ribosyl polymerase (PARP) inhibitors than wild-type cells, indicating that *BRCA1/2* is synthetic lethal with the *PARP* genes (Farmer et al., 2005). PARP consists of a family of 18 proteins and is found in most eukaryotes except yeast (Amé et al., 2004; Herceg & Wang, 2001). The founding member of the PARP family, PARP1, recognizes and binds to single stranded breaks (SSBs) as well as intermediates formed during base excision repair (BER), and subsequently undergoes auto-polyADP-ribosylation (Herceg & Wang, 2001; Horton et al., 2014). The resulting polyADP-ribose polymers on PARP1 then recruit proteins involved in BER, such as DNA polymerase β, XRCC1 and DNA ligase IIIα (Horton et al., 2014). PARP inhibitors hinder the polyADP-ribosylation activity of PARP, thereby leaving PARP1 trapped at damaged DNA and unable to recruit BER proteins to repair SSBs (Horton et al., 2014; Murai et al., 2012). Replication fork stalls when encountering SSBs, resulting in DSBs that are preferentially repaired through HR (Murai et al., 2012). It explains why PARP knockout mice have no negative phenotype and *BRCA1/2* deficiencies sensitize cancer cells to PARP inhibitors (Farmer et al., 2005; Murai et al., 2012; Wang et al., 1995). Although PARP is non-essential, inhibition of PARP is lethal in *BRCA1/2*-deficient cancer cells that have defective HR (Horton et al., 2014). The fact that three PARP inhibitors have been approved by FDA to treat patients with *BRCA1/2*-mutant cancers demonstrates the viability of applying the concept of synthetic lethality as an approach to developing novel cancer therapeutics (Ashworth & Load, 2018). However, clinical data have shown that both innate and acquired resistance to PARP inhibitors develop in patients (Ashworth & Load, 2018). Hence, further studies on other synthetic lethal interactions with *BRCA1/2* genes and alternative ways to target *BRCA1/2*-deficient cancer cells are crucial to cancer therapy.

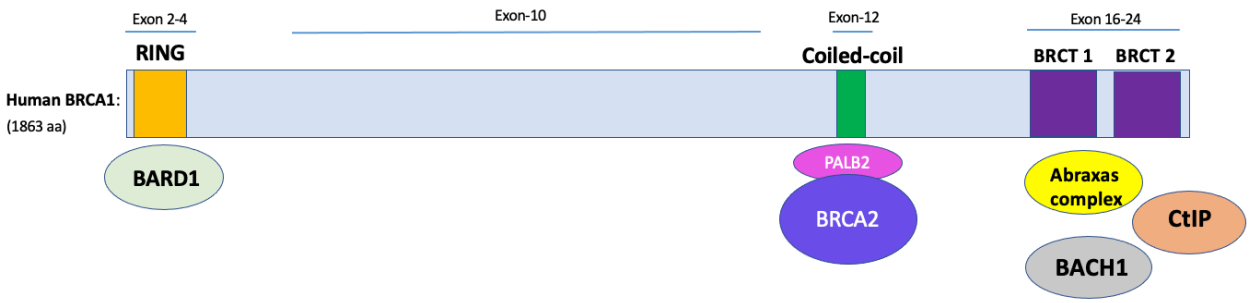

Figure 1.1 Structure and Interacting Proteins of Human BRCA1. The domains of BRCA1 are shown, with the RING (Really Interesting New Gene) domain in yellow, the coiled-coil domain in green and the 2 BRCT (BRCA1 C-terminal) domains in purple. The exons corresponding to each domain of BRCA1 are shown on the top. The binding partners for each domain of BRCA1 are shown in the bottom ovals as BARD1: BRCA1-associated ring domain 1. PALB2: partner and localizer of BRCA2. CtIP: CtBP-interacting protein. BACH1: BRCA1-associated carboxyl-terminal helicase.

1.4 Gene Editing with CRISPR/CAS9 Technology

An isogenic cell line pair that only differs in one gene is useful for validating synthetic lethal interactions between the gene of interest and another non-essential gene (Huang et al., 2020). Precise genome editing to modify the gene of interest can be achieved using clustered regularly interspaced short palindromic repeats(CRISPR)/CRISPR-associated(CAS9) technology. As one of the adaptive immune systems in bacteria, the well-characterized Type II CRISPR system consists of the Cas9 nuclease, the CRISPR RNA (crRNA) complementary to the target DNA sequence as well as the trans-activating crRNA (tracrRNA) required for the maturation of crRNA (Cong et al., 2013; Garneau et al., 2010; Jinek et al., 2012). The crRNA-tracrRNA hybrid directs Cas9 protein to mediate double-stranded breaks (DSBs) at target DNA that matches the guide sequence of crRNA (Cong et al., 2013; Jinek et al., 2012). DSBs induced by Cas9 can be repaired through nonhomologous end joining (NHEJ) that results in indel mutations if a repair template is absent, or through homology-directed repair (HDR) to generate precise and desired editing if a repair template is provided (Ran et al., 2013). Hence, CRISPR/CAS9 technology is a powerful gene editing tool that allows us to knockout genes, correct mutated genes as well as introduce specific mutations at particular locations in the genome.

1.5 Hypothesis and Experimental Approach

Extrapolating from the yeast genetic studies, my MS thesis research project investigates the synthetic lethal interaction between BRCA1 and FEN1 in human cells. A previous graduate student in our lab has shown that *BRCA1*-deficient ovarian cancer cells are more sensitive than *BRCA1*-proficient ovarian cancer cells to SMD154, a drug that inhibits FEN1 (Guo et al., 2020).

Given the genetic and epigenetic heterogeneity among cancer cell lines, the correlative evidence from our previous study does not prove that the loss of BRCA1 alone is sufficient to cause sensitivity to FEN1 inhibitors (Guo et al., 2020). Therefore, the goal of my research is to test the sufficiency of *BRCA1*-mutation in causing FEN1-inhibitor-sensitivity in ovarian cancer cells. The genetic study of the relationship between the BRCA1 and FEN1 will critically evaluate the potential of using FEN1 inhibitors to induce synthetic lethality in *BRCA1*-deficient ovarian cancer.

My MS research project addresses the experimental question of whether mutation of the *BRCA1* gene is necessary and sufficient to cause sensitivity of ovarian cancer cells to SMD2485, another potent FEN1 inhibitor. Correction of the *BRCA1* mutation in the FEN1-inhibitor sensitive UWB1.289 ovarian cancer cells with mutant form of BRCA1 was undertaken to prove necessity of this mutation for sensitivity to SMD2485, and introduction of *BRCA1* mutation in the FEN1-inhibitor resistant OV90 ovarian cancer cells with wild-type BRCA1 was attempted to prove the sufficiency. If the hypothesis that *BRCA1* mutation is the cause of sensitivity to SMD2485 is supported, I would expect the *BRCA1*-corrected UWB1.289 cells to lose the sensitivity to SMD2485, while the *BRCA1-mutant* OV90 cells to gain sensitivity to SMD2485.

The *BRCA1*-deficient UWB1.289 ovarian cancer cell line was derived from a papillary serous ovarian carcinoma of a *BRCA1* germline mutation carrier (*BRCA1*+/-) with loss of the wild-type *BRCA1* allele in the tumor cells (DelloRusso et al., 2007). Specifically, the mutation occurs in exon-10 of BRCA1 where the deletion of a single C (ΔC) at position 43,093,056 of chromosome 17 (GRCh38) leads to a frameshift, resulting in a premature stop codon and eventually nonsense-mediated decay of the mutant *BRCA1*-mRNA (Cunningham et al., 2019; DelloRusso et al., 2007; Tate et al., 2019). The epithelial ovarian cancer cell line OV90 has wild-

type *BRCA1* and was derived from a patient with malignant papillary serous adenocarcinoma (Provencher et al., 2000). CRISPR/Cas9 gene-editing technology was used to achieve the editing of the two ovarian cancer cell lines, and the sensitivities to SMD2485 of parental cells and the corresponding *BRCA1*-edited cells were measured using viability and colony formation assays to determine whether the *BRCA1*-mutation is the cause of sensitivity to FEN1 inhibitors in ovarian cancer cells.

1.6 References

Amé, J., Spenlehauer, C., & Murcia., G. (2004). The PARP superfamily. *BioEssays*, 26(10), 882-893. doi: 10.1002/bies.20085

Asagoshi, K., Tano, K., Chastain, P. D., 2nd, Adachi, N., Sonoda, E., Kikuchi, K., Koyama, H., Nagata, K., Kaufman, D. G., Takeda, S., Wilson, S. H., Watanabe, M., Swenberg, J. A., & Nakamura, J. (2010). FEN1 functions in long patch base excision repair under conditions of oxidative stress in vertebrate cells. *Molecular cancer research : MCR*, *8*(2), 204–215. https://doi.org/10.1158/1541-7786.MCR-09-0253

Ashworth, A., & Lord, C. J. (2018). Synthetic lethal therapies for cancer: what's next after PARP inhibitors? *Nature Reviews Clinical Oncology*, 15(9), 564–576. doi: 10.1038/s41571-018-0055-6

Balakrishnan, L., & Bambara, R. A. (2013). Flap endonuclease 1. *Annual review of biochemistry*, 82, 119–138. doi:10.1146/annurev-biochem-072511-122603

Cong, L., Ran, F. A., Cox, D., Lin, S., Barretto, R., Habib, N., Hsu, P. D., Wu, X., Jiang, W., Marraffini, L. A., & Zhang, F. (2013). Multiplex genome engineering using CRISPR/Cas systems. *Science (New York, N.Y.)*, *339*(6121), 819–823. https://doi.org/10.1126/science.1231143

Cunningham, F., Achuthan, P., Akanni, W. et al. Ensembl 2019, *Nucleic Acids Research*, Volume 47, Issue D1, 08 January 2019, Pages D745-D751, https://doi.org/10.1093/nar/gky1113

Debrauwère, H., Loeillet, S., Lin, W., Lopes, J., & Nicolas, A. (2001). Links between replication and recombination in Saccharomyces cerevisiae: a hypersensitive requirement for homologous recombination in the absence of Rad27 activity. *Proceedings of the National Academy of Sciences of the United States of America*, *98*(15), 8263–8269. https://doi.org/10.1073/pnas.121075598

Dellorusso, C., Welcsh, P. L., Wang, W., Garcia, R. L., King, M. C., & Swisher, E. M. (2007). Functional Characterization of a Novel BRCA1-Null Ovarian Cancer Cell Line in Response to

Ionizing Radiation. *Molecular Cancer Research*, *5*(1), 35–45. doi: 10.1158/1541-7786.mcr-06-0234

Farmer, H., Mccabe, N., Lord, C. J., Tutt, A. N. J., Johnson, D. A., Richardson, T. B., Santarosa, M., Dillon, K. J., Hickson, I., Knights, C., Martin, N. M. B., Jackson, S. P., Smith, G. C. M., & Ashworth, A. (2005). Targeting the DNA repair defect in BRCA mutant cells as a therapeutic strategy. *Nature*, *434*(7035), 917–921. doi: 10.1038/nature03445

Garneau, J. E., Dupuis, M.-È., Villion, M., Romero, D. A., Barrangou, R., Boyaval, P., Fremaux, C., Horvath, P., Magadán, A. H., & Moineau, S. (2010). The CRISPR/Cas bacterial immune system cleaves bacteriophage and plasmid DNA. *Nature*, *468*(7320), 67–71. doi: 10.1038/nature09523

Giaever, G., Chu, A. M., Ni, L., Connelly, C., Riles, L., Véronneau, S., Dow, S., Lucau-Danila, A., Anderson, K., André, B., Arkin, A. P., Astromoff, A., El-Bakkoury, M., Bangham, R., Benito, R., Brachat, S., Campanaro, S., Curtiss, M., Davis, K., Deutschbauer, A., Entian, K.-D., Flaherty, P., Foury, F., Garfinkel, D. J., Gerstein, M., Gotte, D., Güldener, U., Hegemann, J. H., Hempel, S., Herman, Z., Jaramillo, D. F., Kelly, D. E., Kelly, S. L., Kötter, P., LaBonte, D., Lamb, D. C., Lan, N., Liang, H., Liao, H., Liu, L., Luo, C., Lussier, M., Mao, R., Menard, P., Ooi, S. L., Revuelta, J. L., Roberts, C. J., Rose, M., Ross-Macdonald, P., Scherens, B., Schimmack, G., Shafer, B., Shoemaker, D. D., Sookhai-Mahadeo, S., Storms, R. K., Strathern, J. N., Valle, G., Voet, M., Volckaert, G., Wang, C., Ward, T. R., Wilhelmy, J., Winzeler, E. A., Yang, Y., Yen, G., Youngman, E., Yu, K., Bussey, H., Boeke, J. D., Snyder, M., Philippsen, P., Davis, R. W., & Johnston, Mark. (2002). Functional profiling of the *Saccharomyces cerevisiae*genome. *Nature* 418, 387–391. https://doi.org/10.1038/nature00935

Greene, A. L., Snipe, J. R., Gordenin, D. A., & Resnick, M. A. (1999). Functional Analysis of Human FEN1 in Saccharomyces Cerevisiae and Its Role in Genome Stability. *Hum Mol Genet*., 8(12), 2263-73. doi: 10.1093/hmg/8.12.2263.

Godin, S. K., Sullivan, M. R., & Bernstein, K. A. (2016). Novel insights into RAD51 activity and regulation during homologous recombination and DNA replication. *Biochemistry and cell biology = Biochimie et biologie cellulaire*, *94*(5), 407–418. https://doi.org/10.1139/bcb-2016-0012

Gong, Z., Kim, J.-E., Leung, C. C. Y., Glover, J. M., & Chen, J. (2010). BACH1/FANCJ Acts with TopBP1 and Participates Early in DNA Replication Checkpoint Control. *Molecular Cell*, *37*(3), 438–446. doi: 10.1016/j.molcel.2010.01.002

Gudmundsdottir, K., & Ashworth, A. (2006). The roles of BRCA1 and BRCA2 and associated proteins in the maintenance of genomic stability. *Oncogene* 25, 5864–5874. https://doi.org/10.1038/sj.onc.1209874

Hall, J., Lee, M., Newman, B., Morrow, J., Anderson, L., Huey, B., & King, M. (1990). Linkage of early-onset familial breast cancer to chromosome 17q21. *Science*, *250*(4988), 1684–1689. doi: 10.1126/science.2270482

Hartman IV, J.L., Garvik, B., & Hartwell, L.(2001). Principles for the Buffering of Genetic Variation. *Science*, *291*(5506), 1001–1004. doi: 10.1126/science.291.5506.1001

Hartwell, L. H., Szankasi, P., Roberts, C. J., Murray, A. W. & Friend, S. H. (1997). Integrating genetic approaches into the discovery of anticancer drugs. *Science* 278, 1064–1068. doi: 10.1126/science.278.5340.1064

Herceg, Z., & Wang, Z.-Q. (2001). Functions of poly(ADP-ribose) polymerase (PARP) in DNA repair, genomic integrity and cell death. *Mutation Research/Fundamental and Molecular Mechanisms of Mutagenesis*, *477*(1-2), 97–110. doi: 10.1016/s0027-5107(01)00111-7

Horton, J. K., Stefanick, D. F., Prasad, R., Gassman, N. R., Kedar, P. S., & Wilson, S. H. (2014). Base Excision Repair Defects Invoke Hypersensitivity to PARP Inhibition. *Molecular Cancer Research*, *12*(8), 1128–1139. doi: 10.1158/1541-7786.mcr-13-0502

Huang, A., Garraway, L.A., Ashworth, A., & Weber, B. (2020). Synthetic lethality as an engine for cancer drug target discovery. *Nat Rev Drug Discov*, 19, 23–38 . https://doi.org/10.1038/s41573-019-0046-z

Jinek, M., Chylinski, K., Fonfara, I., Hauer, M., Doudna, J. A., & Charpentier, E. (2012). A programmable dual-RNA-guided DNA endonuclease in adaptive bacterial immunity. *Science (New York, N.Y.)*, *337*(6096), 816–821. https://doi.org/10.1126/science.1225829

Kaelin, W. (2005). The Concept of Synthetic Lethality in the Context of Anticancer Therapy. *Nat Rev Cancer* 5, 689–698. https://doi.org/10.1038/nrc1691

Kowalczykowski S. C. (2015). An Overview of the Molecular Mechanisms of Recombinational DNA Repair. *Cold Spring Harbor perspectives in biology*, *7*(11), a016410. https://doi.org/10.1101/cshperspect.a016410

Liu, T., & Huang, J. (2016). DNA End Resection: Facts and Mechanisms. *Genomics, proteomics & bioinformatics*, *14*(3), 126–130. https://doi.org/10.1016/j.gpb.2016.05.002

McManus, K. J., Barrett, I. J., Nouhi, Y., & Hieter, P. (2009). Specific synthetic lethal killing of RAD54B-deficient human colorectal cancer cells by FEN1 silencing. *Proceedings of the National Academy of Sciences of the United States of America*, *106*(9), 3276–3281. https://doi.org/10.1073/pnas.0813414106

Miki, Y., Swensen, J., Shattuck-Eidens, D., Futreal, P. A., Harshman, K., Tavtigian, S., Liu, Q., Cochran, C., Bennett, L. M., Ding, W., Bell, R., Rosenthal, J., Hussey, C., Tran, T., McClure, M., Frye, C., Hattier ,T., Phelps, R., Haugen-Strano, A., Katcher, H., Yakumo, K., Gholami, Z., Shaffer, D., Stone, S., Bayer, S., Wray, C., Bogden, R., Dayananth, P., Ward, J., Tonin, P., Narod, S., Bristow, P. K., Norris, F. H., Helvering, L., Morrison, P., Rosteck, P., Lai, M., Barrett, J. C., Lewis, C., Neuhausen, S., Cannon-Albright, L., Goldgar, D., Wiseman, R., Kamb, A., & Skolnick, M. H. (1994). A strong candidate for the breast and ovarian cancer susceptibility gene BRCA1. *Science*, *266*(5182), 66–71. doi: 10.1126/science.7545954

Morales, J., Li, L., Fattah, F. J., Dong, Y., Bey, E. A., Patel, M., Gao, J., & Boothman, D. A. (2014). Review of poly (ADP-ribose) polymerase (PARP) mechanisms of action and rationale for targeting in cancer and other diseases. *Critical reviews in eukaryotic gene expression*, *24*(1), 15–28. https://doi.org/10.1615/critreveukaryotgeneexpr.2013006875

Murai, J., Huang, S.-Y. N., Das, B. B., Renaud, A., Zhang, Y., Doroshow, J. H., Ji, J., Takeda, S., & Pommier, Y. (2012). Trapping of PARP1 and PARP2 by Clinical PARP Inhibitors. *Cancer Research*, *72*(21), 5588–5599. doi: 10.1158/0008-5472.can-12-2753

Paul, A., & Paul, S. (2014). The breast cancer susceptibility genes (BRCA) in breast and ovarian cancers. *Frontiers in bioscience (Landmark edition)*, *19*, 605–618. https://doi.org/10.2741/4230

Provencher, D. M., Lounis, H., Champoux, L., Tétrault, M., Manderson, E. N., Wang, J. C., Eydoux, P., Savoie, R., Tonin, P. N., & Mes-Masson, A. M. (2000). Characterization of Four Novel Epithelial Ovarian Cancer Cell Lines. *In Vitro Cellular & Developmental Biology - Animal*, *36*(6), 357. doi: 10.1290/1071-2690(2000)036<0357:cofneo>2.0.co;2

Ran, F. A., Hsu, P. D., Wright, J., Agarwala, V., Scott, D. A., & Zhang, F. (2013). Genome engineering using the CRISPR-Cas9 system. *Nature protocols*, *8*(11), 2281–2308. https://doi.org/10.1038/nprot.2013.143

Rosen, E.M. (2013). BRCA1 in the DNA damage response and at telomeres. *Frontiers in genetics*, 4, 85. https://doi.org/10.3389/fgene.2013.00085

Sartori, A. A., Lukas, C., Coates, J., Mistrik, M., Fu, S., Bartek, J., Baer, R., Lukas, J., & Jackson, S. P. (2007). Human CtIP promotes DNA end resection. *Nature*, *450*(7169), 509–514. doi: 10.1038/nature06337

Steichen-Gersdorf, E., Gallion, H. H., Ford, D., Girodet, C., Easton, D. F., DiCioccio, R. A., Evans, G., Ponder, M. A., Pye, C., & Mazoyer, S. (1994). Familial site-specific ovarian cancer is linked to BRCA1 on 17q12-21. *American journal of human genetics*, *55*(5), 870–875.

Sy, S. M., Huen, M. S., & Chen, J. (2009). PALB2 is an integral component of the BRCA complex required for homologous recombination repair. *Proc. Natl. Acad. Sci. U.S.A*. 106, 7155–7160. https://doi.org/10.1073/pnas.0811159106

Takaoka, M., & Miki, Y. (2018). *BRCA1* gene: function and deficiency. *Int J Clin Oncol* 23, 36–44. https://doi.org/10.1007/s10147-017-1182-2

Tarsounas, M., & Sung, P. (2020). The antitumorigenic roles of BRCA1–BARD1 in DNA repair and replication. *Nat Rev Mol Cell Biol*. https://doi.org/10.1038/s41580-020-0218-z

Tate, J. G., Bamford, S., Jubb, H. C., Sondka, Z., Beare, D. M., Bindal, N., Boutselakis, H., Cole, C. G., Creatore, C., Dawson, E., Fish, P., Harsha, B., Hathaway, C., Jupe, S. C., Kok, C. Y., Noble, K., Ponting, L., Ramshaw, C. C., Rye, C. E., Speedy, H. E., Stefancsik, R., Thompson, S. L., Wang, S., Ward, S., Campbell, P. J., & Forbes, S. A. (2019). COSMIC: the Catalogue Of Somatic Mutations In Cancer. *Nucleic acids research*, *47*(D1), D941–D947. https://doi.org/10.1093/nar/gky1015

Tishkoff, D. X., Filosi, N., Gaida, G. M., & Kolodner, R. D. (1997). A Novel Mutation Avoidance Mechanism Dependent on S. cerevisiae RAD27 Is Distinct from DNA Mismatch Repair. *Cell*, *88*(2), 253–263. doi: 10.1016/s0092-8674(00)81846-2

Tong, A.H., Evangelista, M., Parsons, A.B., Xu, H., Bader, G.D., Pagé, N., Robinson, M., Raghibizadeh, S., Hogue, C.W., Bussey, H., Andrews, B., Tyers, M., & Boone, C. *(*2001). Systematic genetic analysis with ordered arrays of yeast deletion mutants. *Science* 294, 2364–2368. doi: 10.1126/science.1065810

Tong, A. H., Lesage, G., Bader, G. D., Ding, H., Xu, H., Xin, X., Young, J., Berriz, G. F., Brost, R. L., Chang, M., Chen, Y., Cheng, X., Chua, G., Friesen, H., Goldberg, D. S., Haynes, J., Humphries, C., He, G., Hussein, S., Ke, L., Krogan, N., Li, Z., Levinson, J. N., Lu, H., Ménard, P., Munyana, C., Parsons, A. B., Ryan, O., Tonikian, R., Roberts, T., Sdicu, A. M., Shapiro, J., Sheikh, B., Suter, B., Wong, S. L., Zhang, L. V., Zhu, H., Burd, C. G., Munro, S., Sander, C., Rine, J., Greenblatt, J., Peter, M., Bretscher, A., Bell, G., Roth, F. P., Brown, G. W., Andrews, B., Bussey, H., & Boone, C. (2004). Global mapping of the yeast genetic interaction network. *Science* 303, 808–813. doi: 10.1126/science.1091317

van Pel, D. M., Barrett, I. J., Shimizu, Y., Sajesh, B. V., Guppy, B. J., Pfeifer, T., McManus, K. J., & Hieter, P. (2013). An evolutionarily conserved synthetic lethal interaction network identifies FEN1 as a broad-spectrum target for anticancer therapeutic development. *PLoS genetics*, *9*(1), e1003254. https://doi.org/10.1371/journal.pgen.1003254

Ward, T.A., McHugh, P.J., & Durant, S.T. (2017). Small molecule inhibitors uncover synthetic genetic interactions of human flap endonuclease 1 (FEN1) with DNA damage response genes. *Plos One*, *12*(6). doi: 10.1371/journal.pone.0179278

Wang, Z. Q., Auer, B., Stingl, L., Berghammer, H., Haidacher, D., Schweiger, M., & Wagner, E. F. (1995). Mice lacking ADPRT and poly(ADP-ribosyl)ation develop normally but are susceptible to skin disease. *Genes & Development*, *9*(5), 509–520. doi: 10.1101/gad.9.5.509

Yu, X., & Chen, J. (2004). DNA damage-induced cell cycle checkpoint control requires CtIP, a phosphorylation-dependent binding partner of BRCA1 C-terminal domains. *Mol Cell Biol* 24:9478–9486. doi: 10.1128/MCB.24.21.9478-9486.2004

Zhan, T., & Boutros, M. (2016). Towards a compendium of essential genes - From model organisms to synthetic lethality in cancer cells. *Critical reviews in biochemistry and molecular biology*, *51*(2), 74–85. https://doi.org/10.3109/10409238.2015.1117053

Zheng, L., Zhou, M., Chai, Q., Parrish, J., Xue, D., Patrick, S. M., Turchi, J. J., Yannone, S. M., Chen, D., & Shen, B. (2005). Novel function of the flap endonuclease 1 complex in processing stalled DNA replication forks. *EMBO reports*, *6*(1), 83–89. https://doi.org/10.1038/sj.embor.7400313

Zheng, L., Jia, J., Finger, L. D., Guo, Z., Zer, C., & Shen, B. (2011). Functional regulation of FEN1 nuclease and its link to cancer. *Nucleic acids research*, *39*(3), 781–794. https://doi.org/10.1093/nar/gkq884

CHAPTER 2 MATERIALS AND METHODS

2.1 Selection of sgRNAs

Broad Institute sgRNA Designer (https://portals.broadinstitute.org/gpp/public/analysis-tools/sgrna-design) was used to generate a list of all potential single-guide RNAs (sgRNAs) for targeting the *BRCA1* gene. sgRNA candidates targeting exon-10 of the *BRCA1* gene were sorted and further selected based on the target sites relative to *BRCA1* mutation site in UWB1.289 cells (position 43,093,056 of chromosome 17, GRCh38), on-target efficacy scores and off-target ranks. For double-cutting and -nicking of *BRCA1*, the relative positions of the sgRNA pairs were also considered.

2.2 Preparation of sgRNA-Cas9 Constructs

The following procedure for making sgRNA expression constructs is derived from the protocol described in the paper of Zhang et al. (Ran et al., 2013). The top and bottom strands of sgRNA oligos for each sgRNA design were annealed and phosphorylated at the 5' ends using T4 PNK. The reaction mixture was subjected to 37˚C for 30 min, 95˚C for 5 min and lastly a ramp-down to 25˚C at a rate of 5˚C/min. The phosphorylated and annealed oligos were diluted 1:200. The pSpCas9(BB)-2A-Puro or pSpCas9n(BB)-2A-Puro vector was digested using Bbsl(Bpil) restriction enzyme and incubated with Tango buffer, DTT and ATP at 37˚C for 1 hour. Then the diluted annealed sgRNA oligos were ligated into the digested vectors using T4 DNA ligase at 37˚C for 5 min and 21˚C for 10 min. The ligation reactions were further treated with PlasmidSafe exonuclease, together with PlasmidSafe buffer (10x) and ATP (10mM), at 37˚C for 30 min followed by 70˚C for 30 min to digest any residual linearized DNA. The ligated products were then transformed into 50 µl Subcloning Efficiency DH5α competent cells (ThermoFisher

Scientific) by heat shock, and 1/10 of the bacteria were spread onto LB plates with ampicillin and incubated overnight at 37˚C. Three bacterial colonies were randomly picked from each plate for each sgRNA design and inoculated into 3 ml LB medium with 100 µg/ml ampicillin. The liquid cultures were shaken at 37˚C at 270 rpm overnight. The plasmids were extracted on the next day using PureLink™ Quick Plasmid Miniprep Kit (ThermoFisher Scientific). The sequence of each colony was verified by sequencing from the U6 promoter using the U6-Fwd primer.

For large-scale plasmid preparation, sequence-verified sgRNA-Cas9 plasmids were transformed into Subcloning Efficiency DH5α competent cells (ThermoFisher Scientific), and the bacteria were spread onto LB plates with ampicillin and incubated overnight at 37˚C. A single bacterial colony was inoculated into 3ml of LB medium with 100 µg/ml ampicillin and grown for 8 hours at 280 rpm at 37˚C. The starter culture was then diluted into 50 ml LB medium with 100 µg/ml ampicillin and shaken at 280 rpm overnight. The plasmids were extracted using the Qiagen Plasmid Midi Kit the next day.

2.3 Restriction Enzyme Digestion of sgRNA-Cas9 Constructs

sgRNA-Cas9 expression constructs were digested with FastDigest Bpil (BbsI) or FastDigest BglII (ThermoFisher Scientific) according to the manufacturer's instructions. Each digestion reaction consisted of 1µl 10X FastDigest Green Buffer, 200 ng plasmid DNA, 0.5 µl FastDigest enzyme and nuclease-free water to a total volume of 10 µl. The reaction mixture was incubated at 37˚C in a heat block for 25 min and the digestion reaction products were directly loaded and run on a 1% agarose gel at 100 v for 1 hour.

2.4 Human Cell Lines

HEK293T cells were maintained in Dulbecco's Modified Eagle's Medium (DMEM) supplemented with 1X Penicillin/Streptomycin and 10% Fetal Bovine Serum (FBS). UWB1.289 cells were maintained in 50% RPMI-1640 Medium and 50% MEGM made of MEBM basal medium and SingleQuot additives (except gentamycin-amphotericin B) supplemented with 3% FBS. OV90 cells were maintained in 50% MCDB 105 medium and 50% Medium 199 supplemented with 15% fetal bovine serum (FBS). Cells were cultured at 37˚C and 5% CO2.

2.5 Transfection by Lipofectamine

Cells were seeded 24 hours before transfection and were transfected using Lipofectamine 3000 (ThermoFisher Scientific), following the company's protocol. For 24-well plate transfection, each 50 µl transfection mixture contains a total of 500 ng DNA, 1µl P3000 Reagent and 1.5 µl Lipofectamine 3000 Reagent in Opti-MEM Medium. For 6-well plate transfection, each 250 µl transfection mixture contains 2500 ng DNA, 5 µL P3000 Reagent and 7.5 µL Lipofectamine 3000 Reagent in Opti-MEM Medium. Puromycin selection of transfected cells was applied at a concentration of 3 µg/ml.

2.6 Transfection by Nucleofection

The nucleofection procedure is derived from the protocol of Amaxa Cell line Optimization Nucleofector Kit (Lonza). For each nucleofection, 1-5 million cells were harvested by trypsinization using 0.25% trypsin-ethylenediaminetetraacetate (EDTA) and centrifuged at 800 rpm for 5 min. The cell pellet was resuspended in 100 µl supplemented Nucleofector Solution V and mixed with plasmid DNA. The entire mixture was transferred into a cuvette and

subjected to T-024, T-020 or X-001 nucleofector program pre-set in the Nucleofector 2b Device (Lonza). After execution, 500 µl prewarmed media was added to the cuvette and the entire sample was gently transferred to a prewarmed plate filled with media for incubation. 2 µg plasmid DNA was used to transfect 1 million cells by nucleofection and 6 µg DNA was used to transfect 5 million cells.

2.7 Fluorescence-activated Cell Sorting (FACS) Analysis

Cells transfected with pmaxGFP or pSpCas9(BB)-2A-GFP plasmids were harvested by trypsinization using 0.25% EDTA and centrifuged at 800 rpm for 5 min. The cell pellet was then resuspended in 1 ml of FACS buffer (0.1% BSA, 1X Glutamax and 10 mM HEPES in PBS) and the suspension was transferred to a FACS tube with filter cap. The sample was analyzed immediately using BD LSRFortessa X-20 machine according to the manufacturer's instructions.

2.8 OV90 Single Cell Cloning

Vector-transfected and pSpCas9(sgRNA)-transfected OV90 cells were harvested from the 24-well plate by trypsinization using 0.25% trypsin-EDTA. Viable cells were counted using TC20 Automated Cell Counter (Bio-Rad). To generate single clones of vector-transfected cells, 1 cell was seeded per well of a 96-well plate. To generate single clones of pSpCas9(sgRNA)-transfected cells, 3 cells were seeded per well of three 96-well plates.

2.9 Genomic DNA Extraction by QuickExtract and Genomic PCR

To extract the genomic DNA from cells on 96-well plates, cells were washed with 180 µl phosphate-buffered saline (PBS) and then added with 10 µl QuickExtract™ DNA Extraction

Solution (Lucigen) per well of 96-well plates. Plates were tapped against the table at each side to evenly spread the solution across the wells, then wrapped in aluminum foil and incubated on a 70˚C hot plate for 6 min. After tapping the plates again for 15 s for each side, the plates were incubated on a 100˚C hot plate for 5 min. 1 µl of DNA was used for each genomic PCR reaction. The PCR reactions were performed with Taq DNA Polymerases (NEB) with the following thermocycling conditions: initial denaturation at 95˚C for 30 s, 33 cycles of 3-step amplification (95˚C for 20 s, 52˚C for 20 s, 68˚C for 20 s) and final extension at 68˚C for 5 min. Genomic PCR products were run on 2% agarose gels at 100 v for 45 min.

2.10 TOPO Cloning and Sequencing for Insert

Fresh genomic PCR products were mixed with the TOPO vector from the TOPO TA Cloning Kits for Sequencing (Invitrogen) at a 4:1 ratio and incubated at room temperature for 5 min. 1 µl of the TOPO cloning reaction was transformed into Subcloning Efficiency DH5α-T1 cells by heat shock, which were then spread onto ampicillin-containing LB plates pre-added with 40 µl of the 40 mg/ml X-gal. The plates were incubated overnight at 37˚C. 6 to 8 light blue colonies were randomly selected per reaction for plasmid purification using PureLink^{TM} Quick Plasmid Miniprep Kit (Invitrogen). The nucleotide sequences of the genomic PCR products were obtained by Sanger sequencing using the M13 Forward (-20) primer.

2.11 Immunoblotting

Cells were collected using a cell scraper in ice-cold 1X PBS, transferred to 15-ml centrifuge tubes and centrifuged at 800 rpm for 5 min at 4˚C. Cell pellets were resuspended in 1 ml of ice-cold PBS, transferred to Eppendorf tubes and centrifuged in an Eppendorf 5415

Centrifuge at max speed for 10 seconds. Cell pellets were lysed in RIPA buffer (ThermoFisher Scientific) with Protease Inhibitor Cocktail (Sigma) and phenylmethanesulfonyl fluoride mixtures for 20 min on ice, sonicated with 10 pulses, and cleared by centrifugation at 14000 rpm for 30 min at 4˚C. Protein concentration was measured by Bio-Rad *DC* Protein Assay. Total cell lysates were separated by SDS-PAGE gel electrophoresis on 4-15% Mini-PROTEAN TGX Precast Protein Gels (Bio-Rad) and the proteins were transferred from mini gels to polyvinylidene fluoride (PVDF) membranes (Bio-Rad) using the HIGH MW transfer program of the Trans-Blot Turbo Transfer System (Bio-Rad). Blot were blocked with 5% nonfat dry milk in 1X TBST (Tris-buffered saline with 0.1% Tween 20) for 1 hour and incubated with primary antibodies against BRCA1 at 1µg/ml (Bethyl Laboratories; A300-000A) or GAPDH at 1µg/ml (Cell Signaling Technology; 2118S) overnight at 4˚C. Blots were washed in 1X TBST three times for 5 min and incubated with horseradish peroxidase (HRP)-conjugated rabbit secondary antibody (Cell Signaling Technology) for 1 hour at room temperature. Blots were washed in 1X TBST three times for 5 min and developed using SuperSignal West Pico PLUS Chemiluminescent Substrate (ThermoFisher Scientific), according to the manufacturer's instructions. Target proteins were detected using a ChemiDoc MP imager (Bio-Rad).

2.12 Measuring SMD2485 IC_{50} Values by MTT assay or CV assay

6000 cells were seeded per well of 96-well plates and incubated overnight. After 24 h, the cells were treated with 0 to 200 µM of the FEN1 inhibitor (SMD2485) in 3-fold serial dilutions for 3 days. The first column of the plates contained only media and the last column of the plates contained cells without any treatment. For MTT assay, cells were added and incubated with 20 µl MTT solution per well for 2 hours. After removing the MTT-containing media completely,

the purple color was dissolved in 150 µl DMSO per well and quantified by measuring the absorbance at 540 nm using the VersaMax Tunable Microplate Reader (VWR). For CV assay, cells were fixed with 200 µl of 100% methanol per well for 10 min at -20˚C and stained with 50 µl crystal violet solution (1% CV in methanol) per well for 30 min at room temperature. The CV solution was then removed and the plates were washed in a container with deionized water until the water was clear. The plates were air-dried with the lid off for 24 hours. The stain was extracted with 10% acetic acid solution (100µl per well) and quantified by measuring the absorbance at 570 nm using the VersaMax Tunable Microplate Reader (VWR). For data processing, the average blank reading was subtracted from the average reading for each drug concentration. The ratios of the average drug-treated readings to the no-drug control reading were calculated and presented as percentage viability, which were then imported into the ATT Bioquest IC_{50} calculator (https://www.aatbio.com/tools/ic50-calculator) to determine the IC_{50} values .

2.13 Measuring SMD2485 IC_{50} Values by Clonogenic Assay

3000 cells were seeded per well of 6-well plates. After 24 hours, cells were treated with 60 µM, 20 µM, 6 µM, 2 µM, 0.6 µM, 0.2 µM of FEN1 inhibitor (SMD2485) or DMSO or left untreated for 3 days. Each treatment condition was performed in three technical repeats. On day 3 after drug addition, the media were replaced with fresh media and the cells were allowed to recover for additional 3 days with media replacement on the second day. Resulting colonies were fixed with 1ml of 100% methanol per well for 10 min at -20˚C and stained with 0.5 ml per well crystal violet solution for 30 min at room temperature. The CV solution was then aspirated and completely washed off using deionized water in a container. The plates were air-dried without

the lid for 24 hours in a drawer. Then the images of plates were taken using the AlphaImager HP System and the colony counts were determined by Fiji using the thresholding previously optimized for the OV90 cell line by Guo et al. (2020). The average colony number from the three technical repeats for each treatment condition was calculated and used to determine the IC_{50} values of SMD2485 by ATT Bioquest IC_{50} calculator (https://www.aatbio.com/tools/ic50-calculator).

2.14 References

Guo, E., Ishii, Y., Mueller, J., Srivatsan., A., Gahman, T., Putnam, C.D., Wang, J., & Kolodner, R.D. (2020). FEN1 endonucleases as a therapeutic target for human cancers with defects in homologous recombination. Proceedings of the National Academy of Sciences, 117(32), 19415-19424. doi: 10.1073/pnas.2009237117

Ran, F. A., Hsu, P. D., Wright, J., Agarwala, V., Scott, D. A., & Zhang, F. (2013). Genome engineering using the CRISPR-Cas9 system. *Nature protocols*, *8*(11), 2281–2308. https://doi.org/10.1038/nprot.2013.143

CHAPTER 3 CORRECTION OF the *BRCA1* MUTATION IN UWB1.289 OVARIAN CANCER CELLS

3.1 Rationale

Previous work from our lab has shown that *BRCA1*-deficient UWB1.289 ovarian cancer cells are hypersensitive to FEN1 inhibitors, such as SMD154 (Guo et al., 2020). However, given the genetic and epigenetic heterogeneity among cancer cell lines, the correlative evidence is not sufficient to prove that the mutation in *BRCA1* is the cause of sensitivity of UWB1.289 cells to FEN1 inhibitors. Other underlying factors besides the *BRCA1*-mutation could have contributed to the observed association between *BRCA1*-mutation and FEN1-dependency (Guo et al., 2020). To prove that the *BRCA1* mutation is necessary to cause sensitivity of UWB1.289 cells to FEN1 inhibitors, I decided to revert the *BRCA1* mutation to wild type in UWB1.289 ovarian cancer cells via CRISPR/Cas9-mediated homology-directed repair (HDR) to compare the sensitivities of *BRCA1*-mutant and *BRCA1*-corrected UWB1.289 cells to the FEN1-inhibitor SMD2485, which is more potent than SMD154 in targeting FEN1. If the loss of BRCA1 is necessary to cause FEN1-inhibitor sensitivity, I would expect the *BRCA1*-corrected UWB1.289 cells to be no longer hypersensitive to FEN1 inhibitors.

3.2 Results

3.2.1 Selection of sgRNAs and Design of Repair Template for Correcting the *BRCA1* Mutation in UWB1.289 Cells

In *BRCA1*-deficient UWB1.289 ovarian cancer cells, *BRCA1* is mutated by the deletion of a single C/G base pair (ΔG/C)in exon-10 (position 43,093,056 of chromosome 17, GRCh38) that results in a frameshift, leading to premature termination of translation and possibly the

nonsense-mediated mRNA decay (Perrin-Vidoz et al., 2002). To correct the *BRCA1* mutation in UWB1.289 cells via CRISPR/Cas9-mediated homology-directed repair (HDR), I planned to introduce double-stranded breaks (DSBs) near the *BRCA1* single nucleotide deletion in UWB1.289 cells through both single-cutting and double-nicking strategies and to facilitate HDR of the DBSs by providing a repair template in the form of single-stranded DNA oligonucleotide (ssODN).

For the single-cutting strategy, I selected a single-guide RNA (sgRNA) that guides the wild-type (WT) Cas9 nuclease for generating a cut within exon-10 at genomic position 43,093,054 (sgRNA054) on chromosome 17 (GRCh38), 2 bp upstream of the *BRCA1* ΔG/C mutation in UWB1.289 cells (Figure 3.1A). Besides its closeness to the target site, sgRNA054 has an on-target efficacy score of 0.6442 that ranks 31st out of the 510 candidate sgRNAs for targeting the *BRCA1* gene, suggesting its higher-than-average on-target cleavage efficiency. On the other hand, sgRNA054 is less specific and more likely to result in off-target cleavage as it has an off-target rank of 242nd in relation to the other 509 sgRNA candidates.

To reduce off-target effects, I also tried a double-nicking strategy using the D10A mutant Cas9 nickase (Cas9n) along with a pair of sgRNAs to mediate a DSB. An aspartate-to-alanine (D10A) mutation inactivates the RuvC catalytic domain of the Cas9 nuclease, resulting in a Cas9 nickase that only cleaves the DNA strand complementary to the sgRNA sequence (Ran, Hsu, Wright, Agarwala, Scott, & Zhang, 2013; Jinek et al., 2012). The selected pair of sgRNAs directs Cas9n to simultaneously generate two single-stranded nicks on different DNA strands of the *BRCA1* locus, one at genomic position 43,093,037 (sgRNA037) and the other at 43,093,070 (sgRNA070) on chromosome 17 (GRCh38), resulting in a DSB around the *BRCA1* mutation in UWB1.289 cells (Figure 3.1B). The two Cas9n-nick sites are both within exon-10 and separated

by 32 bp. Upon nicking, the sgRNA pair creates 32-bp 5' overhangs with an overlap of 2 bp between the guide sequences (i.e. -2 bp offset) which is within the optimal offset range from -4 to 20 bp (Ran, Hsu, Lin, Gootenberg, Konermann, Trevino, Scott, Inoue, Matoba, Y. Zhang, & F. Zhang, 2013). The two sgRNAs target opposite DNA strands with the PAM sequences facing outwards with respect to each other and such PAM-out orientation is more favorable as it results in higher editing efficiency than PAM-in configuration does (Bothmer et al., 2017). The off-target ranks for sgRNA037 and sgRNA070 is 39 and 87 out of the 510 sgRNA candidates, respectively, suggesting that the two sgRNAs have higher targeting specificity and fewer potential offsite targets than most of the sgRNA candidates do. In contrast to the high off-target ranks, both sgRNAs have low on-target cleavage efficiency. sgRNA037 has an on-target efficacy score of 0.4939 that ranks 258th out of the 510 candidate sgRNAs and sgRNA070 has an on-target efficacy score of 0.3396 that ranks 438th out of the 510 candidates.

Thus, the two approaches used to generate DSBs near the *BRCA1* single nucleotide deletion mutation in UWB1.289 cells both have advantages and limitations. The sgRNA054 for the single-cutting strategy is less specific but can result in efficient on-target cleavage at genomic position very close to the *BRCA1* mutation in UWB1.289 cells, while the dual nickase approach along with the paired sgRNAs increases the targeting specificity but has poorer on-target cleavage efficiency. By implementing both strategies, I would be able to identify the approach that results in higher editing efficiency.

In order to correct the *BRCA1* mutation in UWB1.289 cells, I designed a ssODN repair template to facilitate HDR of the DSBs generated by the CRISPR/Cas9 system. The 183nt-long ssODN contains homology arms of 75 nt on each side flanking the two nicked sites at genomic positions 43,093,037 and 43,093,070 of chromosome 17 (GRCh38) as well as a single nucleotide

G added to revert the *BRCA1* single nucleotide deletion mutation in UWB1.289 cells, thereby restoring the wild-type *BRCA1* sequence (Figure 3.1C). The length of homology arms on each side falls within the range of 40 to 90 nt for optimal ssODN design, which has been shown to result in higher HDR efficiency (Okamoto et al., 2019; Ran, Hsu, Wright, Agarwala, Scott, & Zhang, 2013).

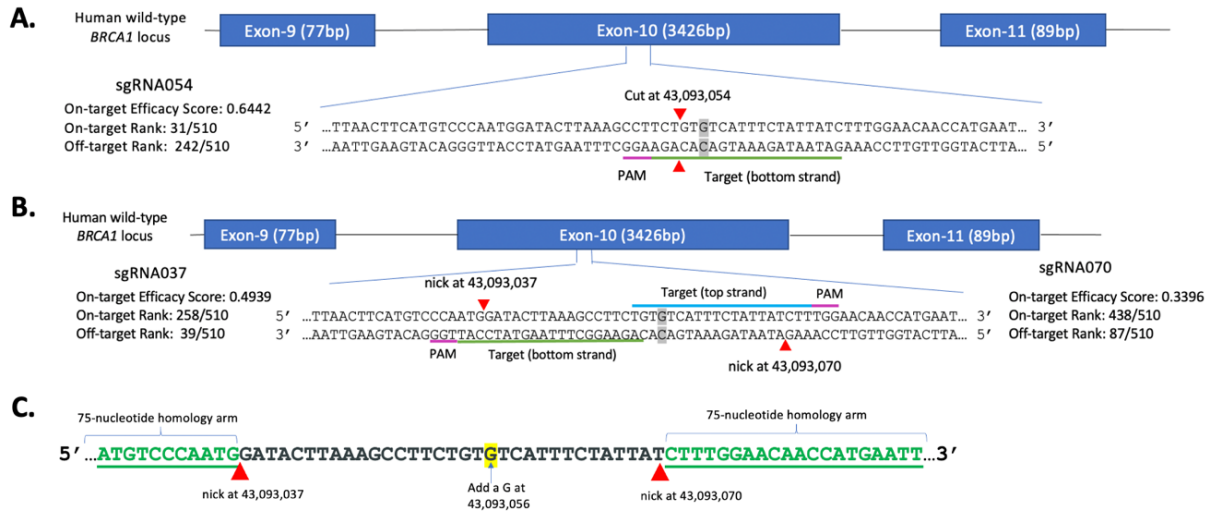

Figure 3.1 Selection of sgRNAs and design of repair template for correcting the *BRCA1* mutation in UWB1.289 Cells. (A and B) Schematic of sgRNA for single-cutting (A), or double-nicking (B) of exon-10 of the *BRCA1* gene. sgRNA054, sgRNA037 and sgRNA070 were selected from the Broad Institute sgRNA Designer (https://portals.broadinstitute.org/gpp/public/analysis-tools/sgrna-design) for cutting near the *BRCA1* single nucleotide deletion (highlighted in gray) mutation in UWB1.289 cells. The on-target efficacy scores and off-target ranks were also taken into consideration. The on-target efficacy score for sgRNA ranges from 0-1.0, where higher scores indicate increased probabilities of cutting. The off-target rank of sgRNA is evaluated in relation to the other 509 candidates for targeting the *BRCA1* gene, with 1 being the most specific. The sgRNA-guided spCAS9-cut site and spCAS9n-nick sites are denoted by red triangles. (C) The single-stranded oligonucleotides repair template. The nucleotide sequence of the homology arms flanking the two nicked sites are in green letters and the nucleotide added to restore the wild-type *BRCA1* sequence is highlighted in yellow.

3.2.2 Construction of sgRNA-expressing Plasmids

Because the sgRNAs selected for single-cutting and double-nicking of *BRCA1* in UWB1.289 cells are designed by the Broad Institute sgRNA Designer based on the wild-type *BRCA1* sequence, modifications to the guide sequences are needed in order for the selected sgRNAs to base-pair with the mutant *BRCA1* sequence in UWB1.289 cells that carries a single nucleotide deletion. Therefore, I added a single nucleotide A to the 5'-end of sgRNA054 and a C to the 5'-end of sgRNA070 to compensate for the deletion of the C/G base pair in UWB1.289 cells (Figure 3.2A). After annealing the top and bottom strands of sgRNA oligos for each sgRNA design, digestion of pSpCas9(BB)-2A-Puro plasmid bearing wild-type Cas9 and pSpCas9(BB)n-2A-Puro plasmid bearing Cas9 nickase mutant with restriction enzyme BbsI allows the replacement of restriction sites with the direct insertion of annealed sgRNA oligos between the U6 promoter and the CRISPR scaffold sequence. The sgRNA054-coding sequence was cloned into the pSpCas9(BB)-2A-Puro vector to generate sgRNA054-Cas9 expression construct and the sgRNA037- and sgRNA070-coding sequences was each cloned into the pSpCas9(BB)n-2A-Puro vector to generate sgRNA037-Cas9n and sgRNA070-Cas9n constructs. For each sgRNA design, sgRNA-Cas9(n) plasmids were isolated from 3 randomly picked bacterial colonies using miniprep and verified by restriction enzyme digestion with BbsI. Successful insertion of sgRNA oligos destroys the BbsI recognition sites, so pSpCas9(BB)/pSpCas9(BB)n-2A-Puro vector with the correct annealed sgRNA oligo insert cannot be cut by BbsI into linear DNA of size 9174 bp and should migrate the same distance as the uncut plasmid DNA on an agarose gel. The gel electrophoresis image shows that the nine sgRNA-Cas9 plasmids digested with BbsI have the same band patterns as the undigested ones (Figure 3.2B). It suggests that none of the sgRNA-Cas9 plasmids were cut by BbsI and all of the constructs contain the sgRNA inserts. The

restriction digestion verified plasmids were further verified by Sanger sequencing, which confirms that the inserted sgRNA oligos have the correct sequences.

Next, I generated large quantities of DNA from one of the three sequence-verified sgRNA-Cas9 plasmids for each sgRNA using midiprep. BbsI digestion of the sgRNA-Cas9 plasmids after large-scale purification did not cut the plasmids into linear DNA, indicating that Cas9(sgRNA054), Cas9n(sgRNA037) and Cas9n(sgRNA070) all have successful insertion of sgRNA oligos (Figure 3.2C). The size of the plasmids was then verified by restriction enzyme digestion with BglII, which is expected to cut the sgRNA-Cas9 plasmids into 9kb-long linear DNA. Gel electrophoresis of the BglII-digested Cas9(sgRNA054), Cas9n(sgRNA037) and Cas9n(sgRNA070) result in clear single bands with size around 9000 bp, indicating that all three sgRNA-Cas9 constructs have the right size (Figure 3.2D). The sequences of Cas9(sgRNA054), Cas9n(sgRNA037) and Cas9n(sgRNA070) plasmids after large-scale preparation were verified again by Sanger sequencing.

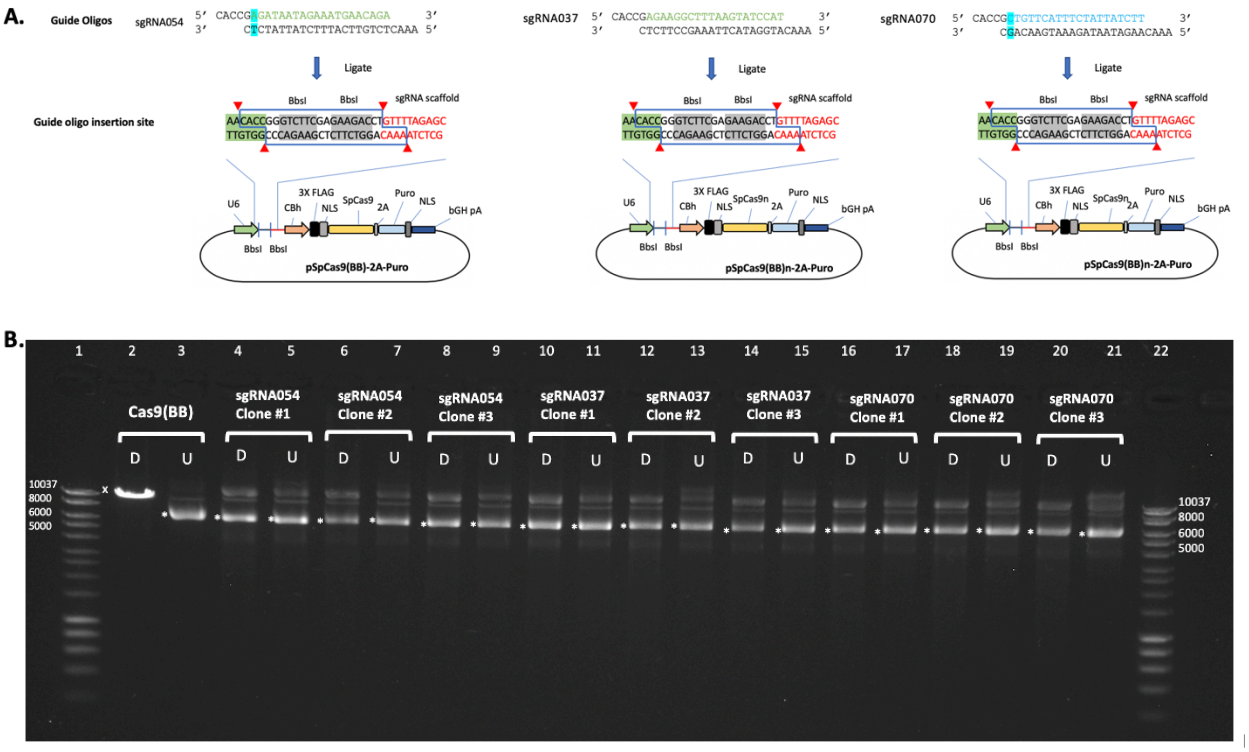

Figure 3.2 Cloning sgRNA oligos into pSpCas9(BB). (A) Schematic of cloning sgRNA oligos into pSpCas9(BB)-2A-Puro or pSpCas9(BB)n-2A-Puro. Nucleotides highlighted in blue are added to the 5'-ends of sgRNA054 and sgRNA070 to compensate for the deletion of the C/G base pair in *BRCA1*-mutant UWB1.289 cells. The sgRNA oligo insertion site is between the U6 promoter and the CRISPR scaffold sequence. The restriction enzyme BbsI is used to cleave the plasmid at two tandem cleavage sites indicated by red triangles and the sequence outlined in blue are replaced with the annealed sgRNA oligos. Nucleotides highlighted in gray are the BbsI recognition sites and the components of the plasmid are shown as CBh: chicken β-actin promoter with hybrid intron. 3X FLAG: 3 tandem FLAG epitope tag (DYKDHD-G-DYKDHD-I-DYKDDDDK). NLS: nuclear localization signal. 2A: 2A peptide from *Thosea asigna* virus capsid protein. Puro: puromycin resistance gene. bGHpA: bovine growth hormone polyadenylation signal. (B) Gel electrophoresis image showing the sgRNA-Cas9 plasmids extracted from 9 bacterial clones with (D) and without (U) BbsI digestion (lanes 4-21). 3 clones were picked for each sgRNA design. pSpCas9(BB)-2A-Puro plasmid with BbsI digestion (lane 2) was used as a negative control and without BbsI digestion (lane 3) was used as a positive control. The band with the expected linearized plasmid size of 9174bp is marked by x and the bands with the expected supercoiled plasmid size are marked by *.

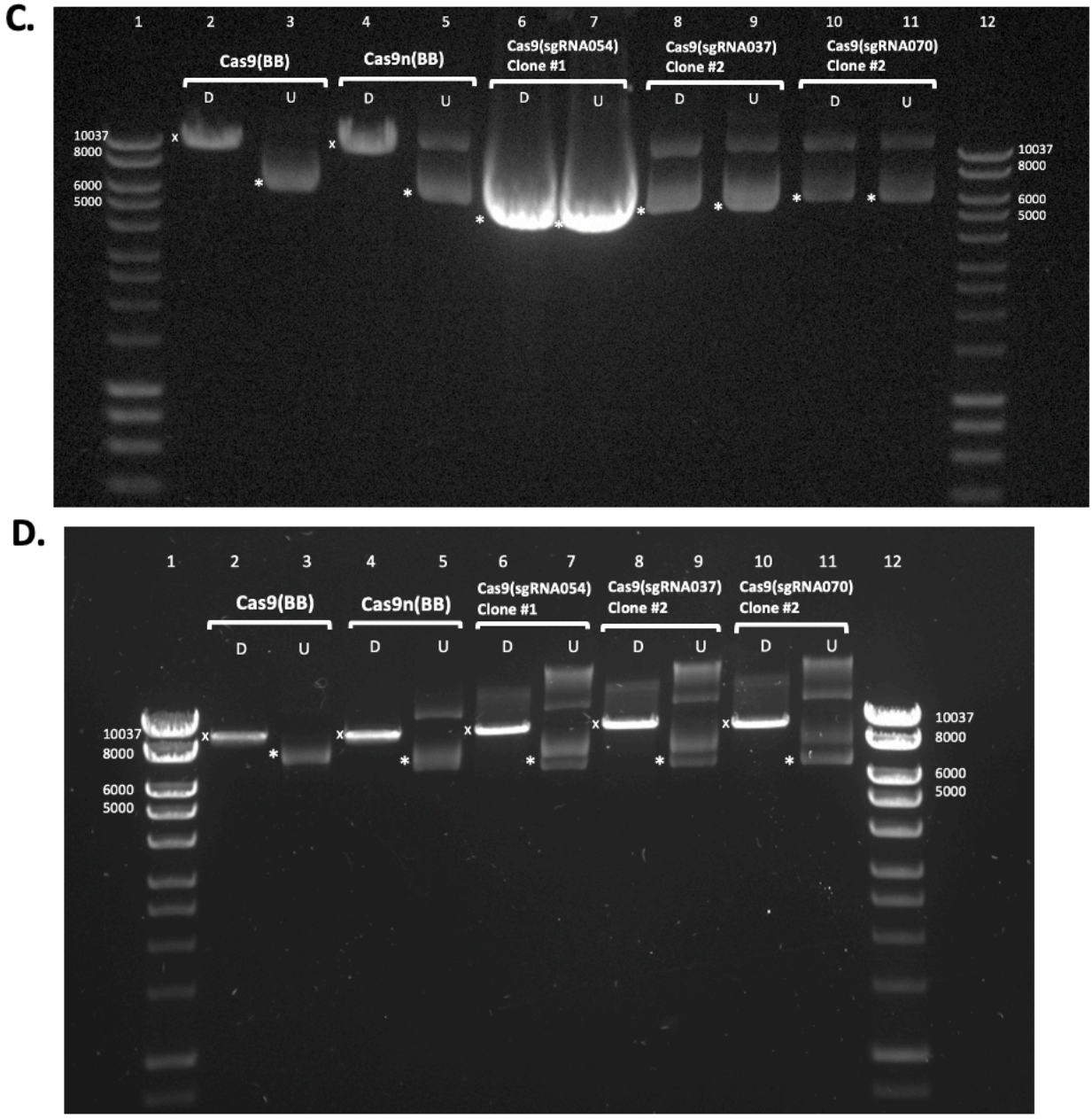

Figure 3.2 Cloning sgRNA oligos into pSpCas9(BB), Continued. (C and D) Gel electrophoresis image showing the 3 selected sgRNA-Cas9 constructs after large scale DNA preparation with and without BbsI digestion (C), or with and without BglII digestion (D). pSpCas9(BB)-2A-Puro and pSpCas9n(BB)-2A-Puro plasmids were used as controls. The band with the expected linearized plasmid size of 9174bp is marked by x and the bands with the expected supercoiled plasmid size are marked by *.

3.2.3 Functional Validation of sgRNA-Cas9 Constructs by HEK293T Transfection

In addition to verifying the correct insertion of sgRNA oligos by restriction enzyme digestion and Sanger sequencing, the ability of the sgRNA-Cas9 constructs to produce CAS9/CAS9n protein and puromycin resistance also needs to be assessed in order to show the plasmids are functional. Therefore, I transfected HEK293T cells, a highly transfectable cell line widely used in research, with the sequence-verified Cas9(sgRNA054), Cas9n(sgRNA037), or Cas9n(sgRNA070) by lipofectamine. A mock transfection in which no plasmid DNA was added was also included. At 24-hour post transfection, cells were split in two into puromycin-containing media. After 48-hour of puromycin treatment, when all mock-transfected cells died, I collected sgRNA-transfected cells and determined the cell count (Figure 3.3). There were 195,750 viable Cas9(sgRNA054)-transfected cells, 320,000 viable Cas9n(sgRNA037)-transfected cells and 322,500 viable Cas9n(sgRNA070)-transfected cells after 48-hr puromycin selection (Table 3.1). Based on the doubling time I have previously determined for HEK293T cells (17 hours) and the viable cell count obtained at 72 h post-transfection, the estimated number of successfully transfected cells out of the 260,000 cells subjected to transfection with each of the sgRNA-Cas9 constructs was calculated. The transfection efficiency of HEK293T cells with pSpCas9(sgRNA054), pSpCas9n(sgRNA037) and pSpCas9n(sgRNA070) was then estimated to be 3.99%, 6.54% and 6.59%, respectively.

HEK293T cells transfected with each of the sgRNA-Cas9/Cas9n plasmids survived the puromycin selection, indicating that the puromycin resistance gene was successfully expressed in the cells by the sgRNA-Cas9/Cas9n plasmids. The presence of puromycin resistance suggests that CAS9/CAS9n were also present because in the sgRNA-Cas9/Cas9n expression constructs, Puro and CAS9/CAS9n are translated from a single mRNA (Ran, Hsu, Wright, Agarwala, Scott,

& Zhang, 2013). Under the control of the RNA polymerase II promoter CBh, which is a modified version of the chicken β-actin (CBA) promoter with hybrid intron from the *CBA* gene and minute virus of mice, the SpCas9/SpCas9n gene appended in-frame with the 2A peptide from *Thosea asigna* virus capsid protein (2A) followed by the Puromycin resistance gene (Cas9/Cas9n-2A-Puro) is transcribed into a single mRNA (Gray et al., 2011; Liu et al., 2017; Ran, Hsu, Wright, Agarwala, Scott, & Zhang, 2013). Two separate polypeptides of SpCAS9/SpCAS9n and Puro are generated during translation when the ribosome fails at forming a peptide bond between a glycine and a proline in 2A (Liu et al., 2017). Therefore, cells that are puromycin resistant after transfection also express CAS9/CAS9n. The successful transfection of HEK293T cells with each of the sgNRA-Cas9/Cas9n constructs suggests that the plasmids are capable of producing CAS9/CAS9n and puromycin resistance, demonstrating the functionality of the constructs.

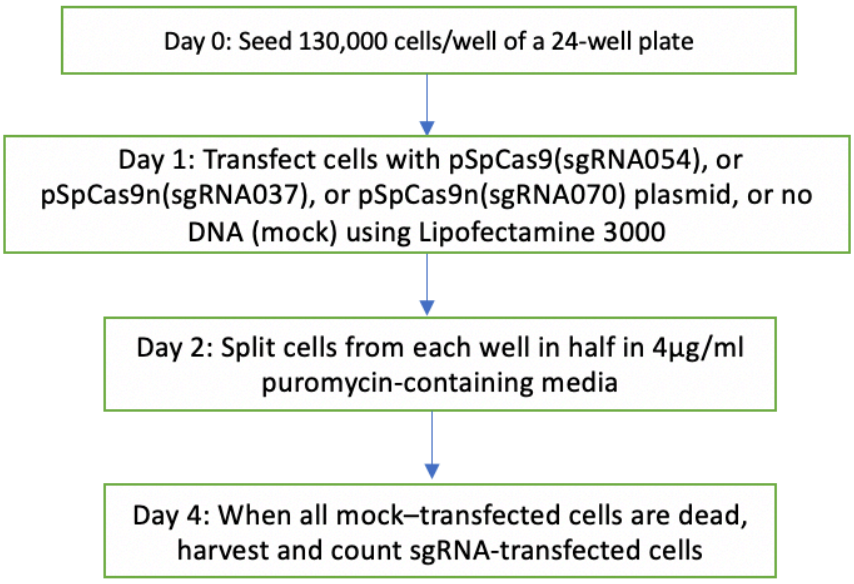

Figure 3.3 Experimental flow chart for functional validation of sgRNA-Cas9 constructs by HEK293T cell transfection.

Table 3.1 Transfection efficiency of HEK293T cells with sgRNA-Cas9 constructs.

	Number of cells seeded for transfection (Day 0)	Expected number of cells ready for transfection (Day 1)	Number of viable transfected cells after puro selection (Day 4)	Estimated number of transfected cells by back-calculation (Day 1)	Transfection Efficiency
pSpCas9(sgRNA054)	130,000	260,000	195,750	10,395	3.99%
pSpCas9n(sgRNA037)	130,000	260,000	320,000	16,994	6.54%
pSpCas9n(sgRNA070)	130,000	260,000	322,500	17,126	6.59%
mock	130,000	260,000	0	0	0

3.2.4 Failure to Obtain Transfected UWB1.289 Cells by Lipofectamine

After validating the sequences and functions of the sgRNA-Cas9 expression constructs, I proceeded to determine the transfection efficiency of UWB1.289 cells with the constructs by lipofectamine. 60,000 UWB1.289 cells were seeded per well of a 24-well plate and transfected with pSpCas9(sgRNA054), pSpCas9n(sgRNA037), or pSpCas9n(sgRNA070) using Lipofectamine 3000 after 24 hours. A mock transfection was also included. At 48-hour post-transfection, cells were treated with puromycin. After 2-day puromycin treatment, only 1 live pSpCas9(sgRNA054)-transfected cell was observed, and the cell did not grow and died after being cultured in fresh growth media for 4 days (Table 3.2).

To determine whether increasing the number of cells being transfected can improve the transfection outcome, I seeded 400,000 UWB1.289 cells per well of a 6-well plate, transfected the cells with pSpCas9(sgRNA054), pSpCas9n(sgRNA037), or pSpCas9n(sgRNA070) using Lipofectamine 3000 after 24 hours and subjected the transfected cells to puromycin selection at 48-hour post-transfection. After 2-day puromycin treatment, when all mock-transfected cells were dead, sgRNA-transfected cells were fed with fresh growth media. One pSpCas9(sgRNA054)-transfected cell and two pSpCas9n(sgRNA070)-transfected cells survived the puromycin selection but did not grow and eventually died after 4 days in fresh media (Table 3.2). It shows that increasing the number of cells subjected to transfection did not lead to more live transfected cells after selection for puromycin resistance. The failure to obtain lipofectamine-transfected cells suggests two possibilities. The first is that UWB1.289 cells are not transfectable by lipofectamine. The second possibility is that transfected UWB1.289 cells cannot survive.

Table 3.2 Failure to obtain transfected UWB1.289 cells by lipofectamine or nucleofection.

Transfection Method	Number of cells seeded for transfection (Day 0)	Number of cells ready for transfection (Day 1)	Number of live cells after puromycin selection (Day 5)	Number of live cells (Day 9)
Lipofectamine 3000	60,000	85,000	1 cell (sgRNA054)	0
Lipofectamine 3000	400,000	560,000	1 cell (sgRNA054) 2 cells (sgRNA070)	0
Nucleofection (X-001)	-	1,000,000	0	0
Nucleofection (X-001)	-	5,000,000	3 cells (sgRNA054) 2 cells (sgRNA037) 3 cells (sgRNA070)	0

3.2.5 pmaxGFP Transfection Efficiency Achieved by Nucleofections of UWB1.289 Cells

To test the first possibility and determine whether UWB1.289 cells can be transfected by other methods, I tried nucleofection, which uses electrical pulses to directly transfer nucleic acids into cells and has been shown to effectively transfect many difficult-to-transfect cell lines (Distler et al., 2005), to transfect 1 million UWB1.289 cells with a 3486 bp-long pmaxGFP plasmid using T-020, T-024 or X-001 nucleofector program. Viable cells were counted and subjected to fluorescence-activated cell sorting (FACS) analysis at 48-hour post nucleofection. A mock nucleofection in which UWB1.289 cells underwent T-024 nucleofector program without the addition of pmaxGFP plasmid was included to set the gates for GFP-negative cells (Figure 3.4A). The cell count shows that only about half of the 1 million mock-transfected cells were viable 48 hours after nucleofection (Table 3.3), indicating that electroporation has some toxic effects on cell viability. The X-001 nucleofector program, which has the shortest execution time, led to the most viable cells but the lowest percentage of GFP-positive cells, overall resulting in the highest number of GFP-positive cells (Table 3.3). Based on the doubling time I previously determined for UWB1.289 cells (48 hours), I estimated the number of GFP-transfected cells on the day of nucleofection and used the number to calculate the transfection efficiency achieved by each program. The X-001 program resulted in a transfection efficiency of 3.9%, which is slightly higher than those from the other two programs (Table 3.3). After FACS analysis, cells that went through each of the nucleofector programs were reseeded and propagated in fresh growth media for another 4 days. T024-transfected and T020-transfected cells continued to die, while X001-transfected cells reattached to the plate and recovered after the FACS analysis. The results suggest that UWB1.289 cells are transfectable by nucleofection.

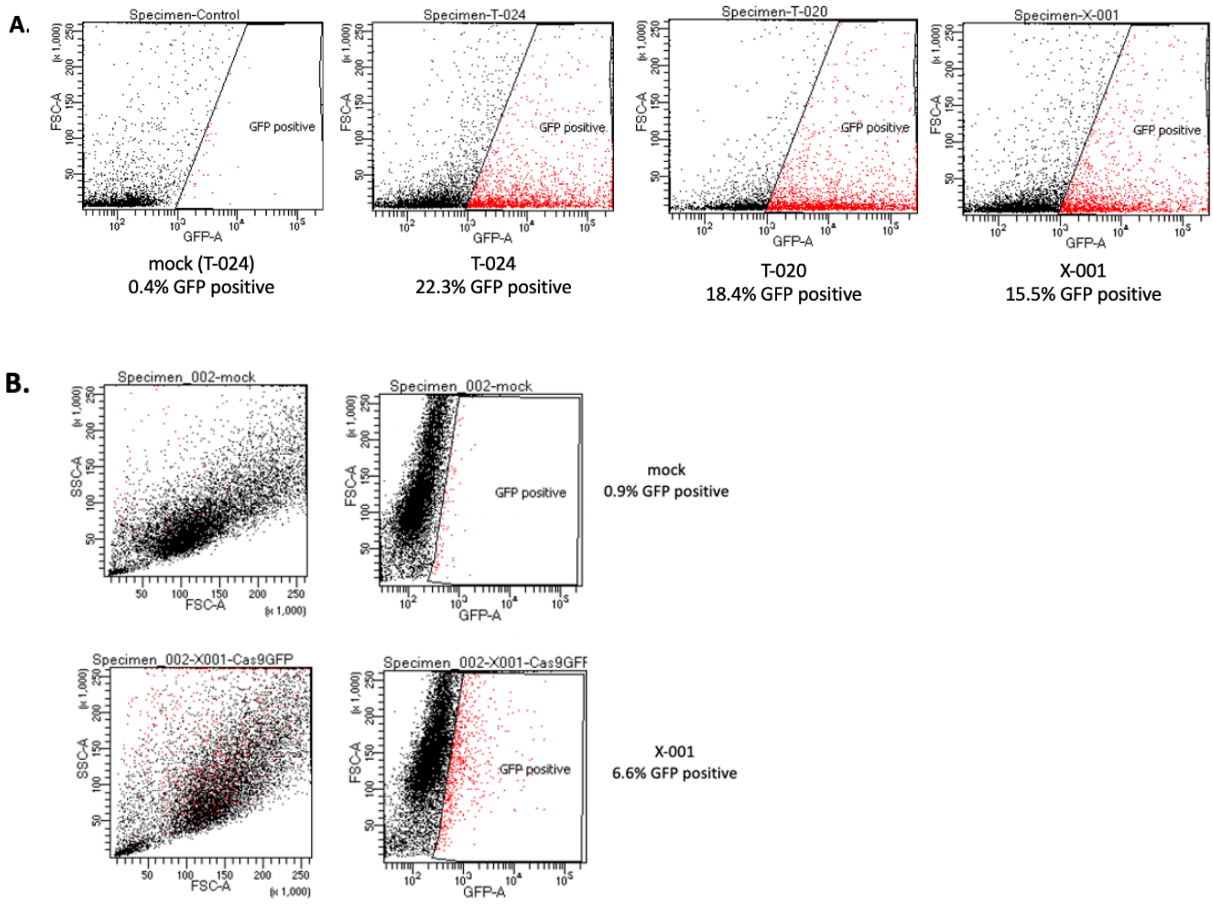

Figure 3.4 Transfection efficiency of UWB1.289 cells from nucleofection with GFP plasmids. (A) FACS profiles of GFP fluorescence (x axis) and forward scatter (y axis) of UWB1.289 cells 48 hours after transfection with pmaxGFP vector using the T-020, T-024 or X-001 Nucleofector program. (B) FACS profiles of UWB1.289 cells 96 hours after transfection with pSpCas9(BB)-2A-GFP plasmid using X-001 Nucleofector program. Dot plots of forward scatter (x axis), side scatter (y axis) and GFP fluorescence (x axis) are shown. The gates for GFP-negative cells were set by the mock-transfected cells, and the percent GFP-positive cells for each nucleofection is shown.

Table 3.3 GFP transfection efficiency achieved by nucleofection of UWB1.289 cells with pmaxGFP vector using 3 nucleofector programs.

Nucleofector Program	Number of cells being transfected (Day 1)	Number of viable cells 48h after nucleofection (Day 3)	% GFP	Number of GFP-positive cells (Day 3)	Estimated number of transfected cells (Day 1)	Transfection Efficiency
T-024	1,000,000	300,000	22.3%	66,900	33,450	3.3%
T-020	1,000,000	414,000	18.4%	73,600	36,800	3.7%
X-001	1,000,000	550,000	15.5%	77,500	38,750	3.9%
Mock (T-024)	1,000,000	590,000	0.4%	2,360	1,180	0.1%

3.2.6 Failure to Obtain pSpCas9(sgRNA)-transfected UWB1.289 Cells by Nucleofection

Given that nucleofection of UWB1.289 cells with the pmaxGFP plasmid resulted in viable GFP-positive cells, I proceeded to transfect 1 million UWB1.289 cells with pSpCas9(sgRNA054), pSpCas9n(sgRNA037) or pSpCas9n(sgRNA070) using the X-001 nucleofector program and selected for transfected cells using puromycin at 48-hour post transfection in order to determine whether nucleofection could also generate viable sgRNA-Cas9 plasmid-transfected cells. The result shows that all of the cells were killed after 2-day puromycin treatment (Table 3.2), suggesting that nucleofection with a 9kb-long pSpCas9(sgRNA) plasmid might be different from a 3kb-long GFP plasmid. As a result, I increased the number of UWB1.289 cells being transfected to 5 million to see whether there would be any viable transfected cells after puromycin selection. I observed 3 live sgRNA054-transfected cells, 2 live sgRNA037-transfected and 3 live sgRNA070-transfected cells after 2-day puromycin treatment, and the few live cells died after being culture in fresh media for 4 days (Table 3.2). The failure to obtain pSpCas9(sgRNA)-transfected UWB1.289 cells suggests that it is possible that UWB1.289 cells are not transfectable by nucleofection when the plasmids are 9kb long.

To find out the transfection efficiency of UWB1.289 cells with plasmids of sizes similar to that of sgRNA-Cas9 construct, I transfected 5 million UWB1.289 cells with the 9288 bp-long pSpCas9(BB)-2A-GFP plasmid using T-020, T-024 or X-001 nucleofector program. A mock nucleofection in which UWB1.289 cells were subjected to the T-024 program but no plasmid DNA was included. At 48-hour post transfection, almost all of the T020- and T024-transfected cells were floating and appeared dead, so I harvested and reseeded them into an 8-chamber slide for detection of GFP-positive cells by fluorescence microscope at 96-hour post transfection. Meanwhile, the live mock-transfected and X001-transfected cells were fed with fresh growth

media and subjected to FACS analysis at 96-hour post transfection (Figure 3.4B). I did not observe any GFP-positive cells treated with T-020 and T-024 programs, suggesting that the two programs were not suitable for transfecting UWB1.289 cells. FACS analysis of the X001-transfected UWB1.289 cells shows that 6.6% of the 1 million viable cells 96 hours after transfection were GFP-positive, and the transfection efficiency was estimated to be 0.33% (Table 3.4), which is much lower than the transfection efficiency of UWB1.289 cells with the 3kb pmaxGFP plasmid. Nevertheless, the results still suggest that UWB1.289 cells are transfectable by nucleofection when the plasmids are 9-kb long.

The observation that there were about 66,000 live GFP-positive UWB1.289 cells at 96-hour post-nucleofection (Table 3.4), while only a few live Cas9(sgRNA)-transfected UWB1.289 cells (Table 3.2) suggests that although there were GFP-positive cells detected by FACS analysis, those transfected cells were in fact not viable and could not be propagated over time. Therefore, the results support the possibility that UWB1.289 cells cannot survive once they acquire exogenous DNA.

Table 3.4 GFP transfection efficiency achieved by nucleofection of UWB1.289 cells with pSpCas9(BB)-2A-GFP plasmid using X-001 nucleofector program.

Nucleofector Program	Number of cells being transfected (Day 1)	Number of viable cells 96h after nucleofection (day 5)	% GFP	Number of GFP-positive cells (Day 5)	Estimated number of transfected cells (Day 1)	Transfection Efficiency
Mock (T-024)	5,000,000	2,700,000	0.9%	24,300	6,075	0.12%
X-001	5,000,000	1,000,000	6.6%	66,000	16,500	0.33%

3.2.7 Sensitivity of UWB1.289 Cells to Exogenous DNA

One possible explanation for why UWB1.289 cells cannot survive once they acquire exogenous DNA is that the plasmids were contaminated with some Penicillin/Streptomycin (P/S)-resistant microbes that killed the UWB1.289 cells. The other possibility is that UWB1.289 cells cannot tolerate exogenous DNA.

To determine whether the death of UWB1.289 cells after transfection was due to microbial contamination of the plasmids, I incubated UWB1.289 cells in P/S-containing media with or without pSpCas9(BB)-2A-GFP plasmid overnight. The microscopic images show that there was no sign of death for cells incubated with GFP plasmid-containing media, suggesting that the GFP plasmids did not contain P/S-resistant contaminants (Figure 3.5). Therefore, the result supports the second possibility that UWB1.289 cells are sensitive to exogenous DNA, which provides a possible explanation for the failure in propagating lipofection- or nucleofection-transfected cells after selection for puromycin resistance.

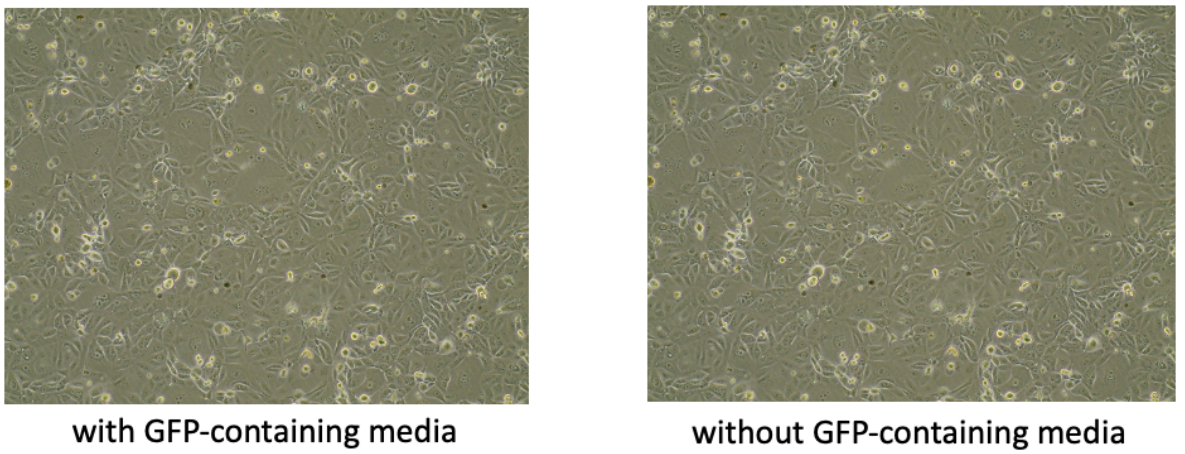

Figure 3.5 Microscopic images of UWB1.289 cells incubated in GFP plasmid-containing media or regular growth media.

3.3 References

Bothmer, A., Phadke, T., Barrera, L. A., Margulies, C. M., Lee, C. S., Buquicchio, F., Moss, S., Abdulkerim, H. S., Selleck, W., Jayaram, H., Myer, V. E., & Cotta-Ramusino, C. (2017). Characterization of the interplay between DNA repair and CRISPR/Cas9-induced DNA lesions at an endogenous locus. *Nature communications*, *8*, 13905. https://doi.org/10.1038/ncomms13905

Distler, J. H., Jüngel, A., Kurowska-Stolarska, M., Michel, B. A., Gay, R. E., Gay, S., & Distler, O. (2005). Nucleofection: a new, highly efficient transfection method for primary human keratinocytes*. *Experimental dermatology*, *14*(4), 315–320. https://doi.org/10.1111/j.0906-6705.2005.00276.x

Gray, S. J., Foti, S. B., Schwartz, J. W., Bachaboina, L., Taylor-Blake, B., Coleman, J., Ehlers, M. D., Zylka, M. J., McCown, T. J., & Samulski, R. J. (2011). Optimizing promoters for recombinant adeno-associated virus-mediated gene expression in the peripheral and central nervous system using self-complementary vectors. *Human gene therapy*, *22*(9), 1143–1153. https://doi.org/10.1089/hum.2010.245

Guo, E., Ishii, Y., Mueller, J., Srivatsan., A., Gahman, T., Putnam, C.D., Wang, J., & Kolodner, R.D. (2020). FEN1 endonucleases as a therapeutic target for human cancers with defects in homologous recombination. Proceedings of the National Academy of Sciences, 117(32), 19415-19424. doi: 10.1073/pnas.2009237117

Jinek, M., Chylinski, K., Fonfara, I., Hauer, M., Duodna, J., & Charpentier, E. (2012). A Programmable Dual-RNA-Guided DNA Endonuclease in Adaptive Bacterial Immunity. *Science, 337*(6096), 816-821. DOI: 10.1126/science.1225829

Liu, Z., Chen, O., Wall, J.B.J., Zheng, M., Zhou, Y., Wang, L., Vaseghi, H., Qian, L., & Liu, J. (2017). Systematic comparison of 2A peptides for cloning multi-genes in a polycistronic vector. *Sci Rep,* 7(2193).

Okamoto, S., Amaishi, Y., Maki, I., Enoki, T., & Mineno, J. (2019). Highly efficient genome editing for single-base substitutions using optimized ssODNs with Cas9-RNPs. *Scientific Reports, 9*(4811). https://doi.org/10.1038/s41598-019-41121-4

Perrin-Vidoz, L., Sinilnikova, O. M., Stoppa-Lyonnet, D., Lenoir, G. M., & Mazoyer, S. (2002). The nonsense-mediated mRNA decay pathway triggers degradation of most BRCA1 mRNAs bearing premature termination codons. Human molecular genetics, 11(23), 2805–2814. https://doi.org/10.1093/hmg/11.23.2805

Ran, F. A., Hsu, P. D., Lin, C. Y., Gootenberg, J. S., Konermann, S., Trevino, A. E., Scott, D. A., Inoue, A., Matoba, S., Zhang, Y., & Zhang, F. (2013). Double nicking by RNA-guided CRISPR Cas9 for enhanced genome editing specificity. *Cell*, *154*(6), 1380–1389. https://doi.org/10.1016/j.cell.2013.08.021

Ran, F. A., Hsu, P. D., Wright, J., Agarwala, V., Scott, D. A., & Zhang, F. (2013). Genome engineering using the CRISPR-Cas9 system. *Nature protocols*, *8*(11), 2281–2308. https://doi.org/10.1038/nprot.2013.143

CHAPTER 4 *BRCA1* KNOCKOUT IN OV90 OVARIAN CANCER CELLS

4.1 Rationale

Previous study from our lab has shown that *BRCA1*-deficient ovarian cancer cells are much more sensitive than *BRCA1*-proficient ovarian cancer cells to FEN1 inhibitors, such as SMD154 (Guo et al., 2020). Although the result demonstrates a strong correlation between the loss of *BRCA1* and FEN1-inhibitor-sensitivity, it suggests but does not prove that *BRCA1* mutation is the cause of sensitivity to FEN1 inhibitors. Given the complexities of biological systems and the genetic and epigenetic variations among cell lines from the same cancer type, or even among cells within one cancer cell line, other underlying factors besides *BRCA1*-mutation could have also contributed to the observed association between *BRCA1*-mutation and FEN1-dependency (Guo et al., 2020). To prove that *BRCA1* mutation is sufficient to cause sensitivity to FEN1 inhibitors, I used CRISPR/Cas9 gene editing technology to knockout *BRCA1* in a *BRCA1*-wild type ovarian cancer cell line, OV90, so as to compare the sensitivities of *BRCA1*-wt and *BRCA1*-mutant OV90 cells to the FEN1-inhibitor SMD2485, which is more potent than SMD154 in targeting FEN1.

4.2 Results

4.2.1 Selection of sgRNAs for Double-Cutting of *BRCA1* in OV90 Cells

According to the Catalogue of Somatic Mutations in Cancer (COSMIC) (Tate et al., 2019), the *BRCA1* mutation in FEN1-inhibitor-sensitive UWB1.289 ovarian cancer cells is a single C/G base pair deletion in exon-10 (position 43,093,056 of chromosome 17, GRCh38) resulting in a frameshift that leads to a mRNA transcript harboring premature stop codon, which is often degraded by nonsense-mediated mRNA decay (Perrin-Vidoz et al., 2002). To model the

BRCA1 frameshift mutation of UWB1.289 cells in OV90 ovarian cancer cells, I selected a pair of single-guide RNAs (sgRNAs) that direct *S. pyogenes* Cas9 (SpCas9) for cutting near 43,093,056, at genomic positions 43,093,157 (sgRNA157) and 43,093,209 (sgRNA209) on chromosome 17 (GRCh38) (Figure 4.1A). The two Cas9-cut sites are both within exon-10 of *BRCA1* and separated by 52 bp. The Broad Institute sgRNA Designer calculated the on-target efficacy scores for sgRNA157 and sgRNA209 based on the "Azimuth_2.0" model to be 0.6231 and 0.6322, respectively, which are higher than 0.4824, the average on-target efficacy score of all 510 candidates for targeting the *BRCA1* gene. In regard to off-target effects, sgRNA157 and sgRNA209 rank 201st and 197th out of the 510 sgRNA candidates, showing that the two selected sgRNAs are not the most specific guides, but are with higher-than-average cleavage efficiency. Furthermore, the two sgRNAs are in the more favorable PAM-out orientation for double cutting as they do not compete with each other for hybridization to the same DNA strand (Bothmer et al., 2017).

After annealing, each of the sgRNA-coding oligos was cloned into the pSpCas9(BB)-2A-Puro vector to generate two targeting constructs: sgRNA157-Cas9 and sgRNA209-Cas9 (Figure 4.1B). In these constructs, the RNA polymerase III promoter for human U6 snRNA (U6) drives the transcription of sgRNA-CRISPR scaffold RNA (Cong et al., 2013). The RNA polymerase II promoter CBh, which is a modified version of the chicken β-actin (CBA) promoter with hybrid intron from the *CBA* gene and minute virus of mice, is used to transcribe SpCas9, with the bovine growth hormone polyadenylation signal (bGHpA) to terminate transcription and polyadenylate the SpCas9 RNA (Gray et al., 2011; Goodwin & Rottman, 1992). In pSpCas9(BB)-2A-Puro, the N-terminus of SpCas9 open reading frame is fused to a 3 tandem FLAG epitope tag (3X FLAG) made up of 22 amino acids (DYKDHD-G-DYKDHD-I-

DYKDDDDK) for immune-detection with anti-FLAG antibody (Zhang et al., 2001), followed by a nuclear localization signal of SV40 large T antigen (NLS) for import into cell nuclei (Cong et al., 2013). The C-terminus of the 3XFLAG-NLS-Cas9 is then appended in-frame with the 2A peptide from *Thosea asigna* virus capsid protein (2A) followed by the Puromycin resistance gene which also contains an NLS and allows for the selection of transfected cells (Liu et al., 2017; Ran et al., 2013). The 2A peptide is a self-cleaving peptide that results from ribosome skipping a peptide bond between a glycine and a proline in 2A during translation, yielding two separate polypeptides of SpCAS9 and Puro from a single mRNA (Liu et al., 2017).

After transforming sgRNA157-Cas9 and sgRNA209-Cas9 into competent cells, I picked 3 bacterial colonies per construct for plasmid purification and verified the plasmids by restriction enzyme digestion and Sanger sequencing. All plasmids were shown to contain the correct insert of sgRNA oligos, indicating the constructs were correctly assembled.

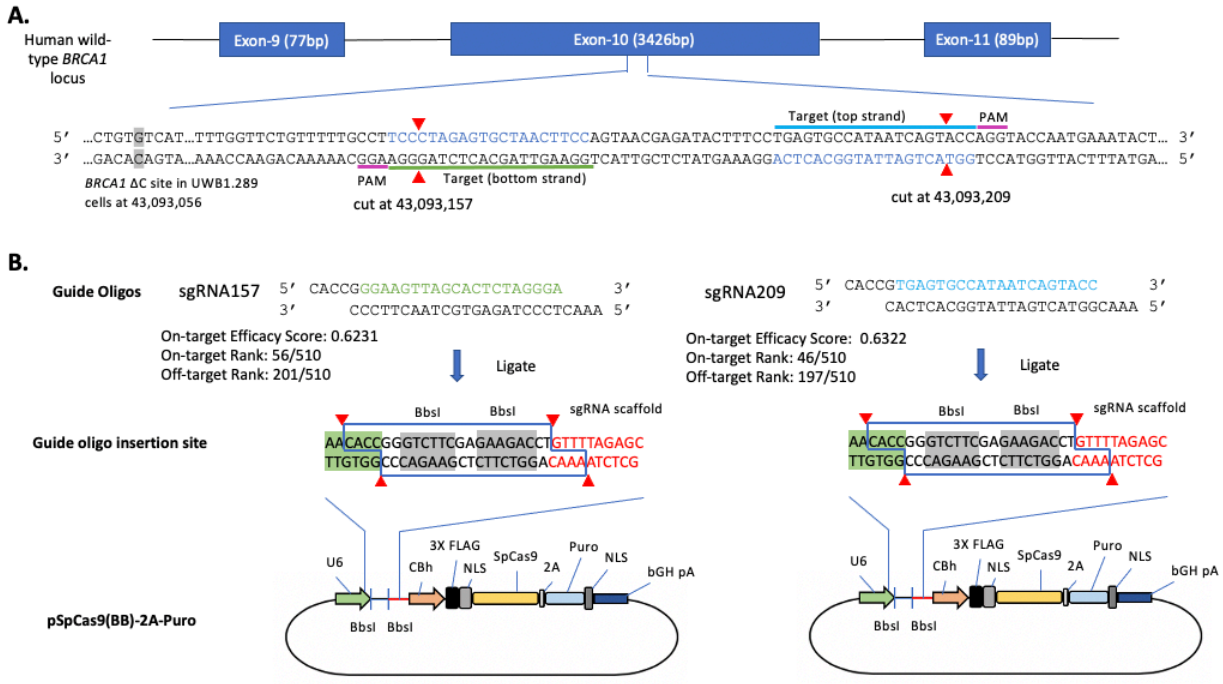

Figure 4.1 Selection of sgRNAs for double-cutting of *BRCA1* in OV90 cells. (A) Schematic of sgRNA targets in exon-10 of the *BRCA1* gene: sgRNA157 and sgRNA209 were selected from the Broad Institute sgRNA Designer (https://portals.broadinstitute.org/gpp/public/analysis-tools/sgrna-design) based on target sites relative to *BRCA1* mutation site in UWB1.289 cells as well as the on-target efficacy scores and off-target ranks. The on-target efficacy score for sgRNA ranges from 0-1.0, where higher scores indicate increased probabilities of cutting. The off-target rank of sgRNA is evaluated in relation to the other 509 candidates for targeting the *BRCA1* gene, with 1 being the most specific sgRNA. The sgRNA-guided spCAS9-cut sites are denoted by red triangles. The two cut sites are oriented in the more favorable PAM-out configuration and separated by 52bp. (B) Schematic of cloning sgRNA oligos into pSpCas9(BB)-2A-Puro: The sgRNA oligo insertion site is between the U6 promoter and the CRISPR scaffold sequence. The restriction enzyme BbsI is used to cleave the plasmid at two tandem cleavage sites indicated by red triangles and the sequence outlined in blue are replaced with the annealed sgRNA oligos. Nucleotides highlighted in gray are the BbsI recognition sites and the components of the plasmid are shown as CBh: chicken β-actin promoter with hybrid intron. 3X FLAG: 3 tandem FLAG epitope tag (DYKDHD-G-DYKDHD-I-DYKDDDDK). NLS: nuclear localization signal. 2A: 2A peptide from *Thosea asigna* virus capsid protein. Puro: puromycin resistance gene. bGHpA: bovine growth hormone polyadenylation signal.

4.2.2 Selection of OV90 Clones with Edited *BRCA1* by Genomic PCR

Next, I transfected OV90 cells with the sequence-verified pSpCas9(sgRNA157) and pSpCas9(sgRNA209) plasmids at equimolar ratios by lipofectamine and subjected the cells to puromycin selection at 24 h post-transfection. A pSpCas9(BB)-2A-Puro vector transfection and a mock transfection of OV90 cells were also included. After 48-hour of puromycin treatment, when all mock-transfected cells died, vector- and pSpCas9(sgRNA)-transfected cells were propagated in fresh media without puromycin for another two days before single cell cloning in 96-well plates. The plates were fed with fresh media every 2 days for 11 days. During this time, any clones that grew to a size of 50-100 cells were trypsinized, transferred to 48-well pates, and further expanded over a 3-week period of successive transfer ending with 10-cm plates. 22 vector-transfected clones were identified from the 96-well plate and 3 of them were transferred to 48-well plate (Day 0), expanded to 12-well plate on Day 8, then to 6-well plate on Day 13 and finally to 10-cm plates on Day 16. A total of 72 pSpCas9(sgRNA)-transfected clones were trypsinized from the three 96-well plates and split into two sets of three 96-well plates which were fed every day for another 7 days (Figure 4.2A).

The genomic DNA of the 72 sgRNA-transfected clones were then extracted from one set of the 96-well plates and amplified using polymerase chain reaction (PCR) in order to screen the sgRNA-transfected clones for the expected 52-bp deletion in *BRCA1*. The expected length of the genomic PCR products from the wild-type *BRCA1* allele is 276 bp and from the edited *BRCA1* allele that resulted from the double-cutting by the two sgRNAs is 224 bp. The genomic PCR products were separated using gel electrophoresis for the detection of bands with wild-type size or edited size. Figure 4.2B is a representative gel electrophoresis image showing the genomic PCR products from 11 sgRNA-transfected OV90 clones. The absence of bands in the water

control lane indicates that there was no contamination of PCR reagents. The genomic DNA from UWB1.289 cells was used as a positive control because its PCR product produced a strong and clear band with wild-type size on the gel. Based on the image, clones 3C8, 3H8, 3D10, 3H10, 3A11 and 3C11 have one band at 276 bp and the other at 224 bp, indicating only one *BRCA1* allele was edited in these clones. Clone 3H9 has a single 276 bp band, indicating neither of the *BRCA1* alleles were edited. There is no visible band with either the expected wild-type size or the edited size in clone 3E9, indicating no PCR product was generated probably due to insufficient amount of genomic DNA in the PCR reaction. Clones 3B12, 3D12 and 3E12 have a single 224 bp band, indicating both *BRCA1* alleles are edited. Out of the 72 sgRNA-transfected clones screened, 22 clones have a single 224 bp band and were selected for sequence analysis and further expansion.

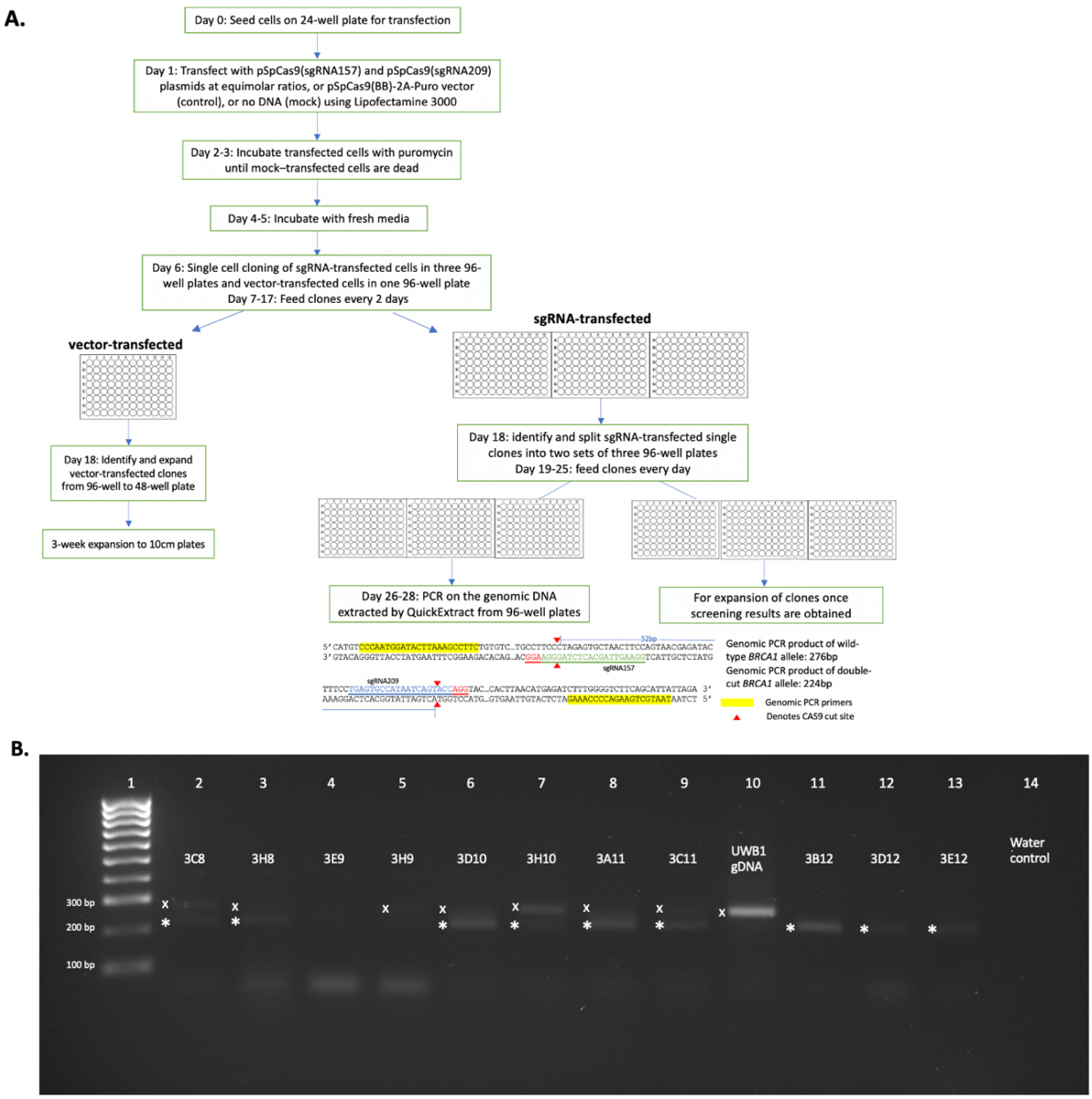

Figure 4. 2 Editing *BRCA1* in OV90 cells by CRIPSR/CAS9. (A) Flow chart of experimental strategy. (B) Representative gel electrophoresis image showing the genomic PCR products from 11 OV90 clones (lanes 2-9, 11-13). Lane 10 is a positive control that uses genomic DNA from UWB1.289 cells because it gave a brighter band at the size of the wild-type *BRCA1* allele than OV90 cells did, and lane 14 is water control. The band with the expected wild-type size of 276 bp is marked by x and the band with the expected edited size of 224 bp is marked by *. Clones 3B12, 3D12, 3E12 (lanes 11-13), each with a single 224 bp band, were picked for further analysis.

4.2.3 Sequence Analysis of the Edited *BRCA1* Alleles in OV90 Clones

To determine the nucleotide sequences of the edited *BRCA1* alleles, the genomic PCR fragments from 12 sgRNA-transfected OV90 clones, each with a single 224 bp band, were cloned into the TOPO vector and transformed into competent bacteria followed by selection for pale-blue colonies on X-gal plates. The PCR-TOPO plasmids were then purified from bacterial colonies and sequenced (Figure 4.3A). The TOPO-cloning data and the characterization of the edited *BRCA1* alleles in the 12 selected clones are summarized in Table 4.1. The "number of TOPO-clones sequenced" refers to the number of bacterial colonies picked for analysis. Of those sequenced, some or all were found to contain the expected sequences of the forward and reverse PCR primers and were approximately 220 bp in length. The number of edited alleles denotes the number of distinct sequences obtained from each OV90 clone analyzed. Each different sequence is counted as one allele for each OV90 clone. The results showed that 10 of the 12 clones had two edited *BRCA1* alleles, while the other 2 clones had a single edited *BRCA1* allele. An allele is considered hypomorphic (H) if it contains a small in-frame deletion, and null (N) if it introduces a premature termination codon. The results showed that, out of the 12 OV90 clones analyzed, none contained wild-type *BRCA1* allele, 7 had one hypomorphic allele and one null allele (H/N), 3 clones had two hypomorphic alleles (H/H), and 2 clones contained only null alleles (N/N).

Aligning the edited sequences with that of the wild type sequence showed different outcomes following Cas9 cutting (Figure 4.3B). Clone 2E6 had two different edited *BRCA1* alleles, one with a 51-nucleotide deletion and the other with the expected 52-nucleotide deletion. Clone 1A9 had a single edited *BRCA1* allele with a 51-nucleotide deletion. Clone 1C8 had a single edited *BRCA1* allele with the expected 52-nucleotide deletion. Clone 2H8 has two different *BRCA1* alleles, one with a 40-nucleotide deletion and an insertion of T at the

sgRNA209 cut site and the other with the expected 52-nucleotide deletion. The predicted amino acid sequences of the edited BRCA1 coding sequences are summarized in Figure 4.3C, showing small in-frame deletions (H-alleles) and premature termination (N-alleles). The edited *BRCA1* allele with the 51-nucleotide deletion in clones 2E6 and 1A9 was predicted to restore the wild-type *BRCA1* reading frame and generate BRCA1 protein with a 17-amino acid in-frame deletion. The *BRCA1* allele with the expected 52-nucleotide deletion in clones 2E6, 1C8 and 2H8 was predicted to introduce a premature stop codon and the resulting BRCA1 amino acid sequence was 1079-amino acid shorter than the full length of wild-type BRCA1 protein (1863 amino acids). The *BRCA1* allele with the 40-nucleotide deletion in clone 2H8 was predicted to introduce a premature termination codon, resulting in a loss of 1088 amino acids in the BRCA1 amino acid sequence. Therefore, clone 2E6 had one hypomorphic allele and one null allele (H/N), clone 1A9 had two hypomorphic alleles (H/H), and clones 1C8 and 2H8 contained only null alleles (N/N).

Once the sequences of the edited *BRCA1* alleles were obtained, OV90 clones 2E6, 1C8, 1A9 and 2H8 were transferred from the duplicate set of the 96-well plates to the 48-well plate and further expanded over the next 20-40 days depending on the growth rates of each clone until there were enough cells for drug-sensitivity tests and protein analysis.

Table 4.1 Summary of the analyses of edited *BRCA1* alleles

Clone	Number of TOPO-clones sequenced	Number of clones containing the expected PCR product	Number of edited alleles	Nature of Mutations Hypomorph (H): small in-frame deletion Null (N): premature termination
1B10	6	4	2	H/N
1E11	4	3	2	H/N
1C8	7	7	1	N/N
1A9	7	6	1	H/H
1F10	8	4	2	H/H
2F1	6	3	2	H/N
2D3	6	6	2	H/N
2E6	6	6	2	H/N
2H8	6	2	2	N/N
3B12	6	5	2	H/N
3D12	6	3	2	H/H
3E12	6	3	2	H/N

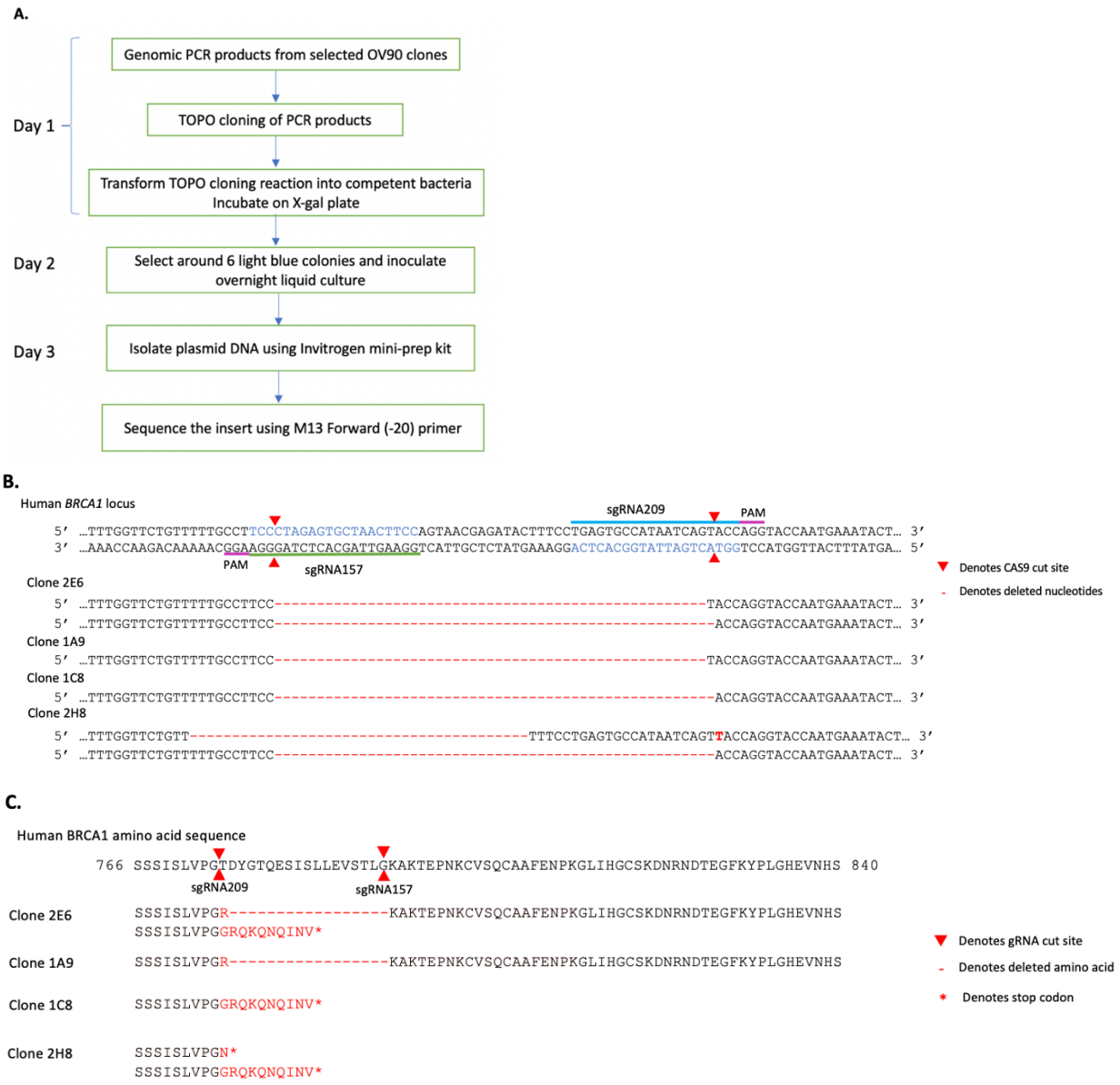

Figure 4.3 Sequencing the edited *BRCA1* alleles in OV90 clones. (A) Experimental flow chart for sequence analysis. (B) Nucleotide sequences of the genomic PCR products from the edited *BRCA1* in selected OV90 clones. (C) Predicted amino acid sequences from each of the edited *BRCA1* alleles in selected OV90 clones. The wild-type BRCA1 amino acid sequence is in black letters. The predicted amino acids are in red letters and the missing amino acids are represented by dashed lines. Premature termination is marked by a red asterisk.

4.2.4 Sensitivity to FEN1 Inhibitor in Selected OV90 Clones

To determine whether *BRCA1*-null OV90 cells are sensitive to FEN1-inhibitor SMD2485, the two *BRCA1*-null OV90 clones 1C8 (N/N) and 2H8 (N/N), together with clones A6 (vector-transfected), 2E6 (H/N) and 1A9 (H/H), each with a different *BRCA1*-genotype, were chosen for the short-term MTT [3-(4,5-dimethylthiazol-2-yl)-2,5-diphenylte-trazolium bromide] assay or the crystal violet (CV) assay to measure the sensitivity of different OV90 clones to SMD2485 after treating cells with 0 to 200μM SMD2485 in 3-fold dilutions for 3 days (Figure 4.4A). Given that the MTT assay measures mitochondrial activity and in some cell lines, the level of oxidative metabolism may or may not track with cell viability, thus, it is necessary to use a second method, the CV staining assay that stains cellular proteins fixed to the culture wells, to compare with the results from MTT assay (van Meerloo et al., 2011; Hongo et al., 1986). Figure 4.4D illustrates the average half maximal inhibitory concentration (IC_{50}) of SMD2485 for clones A6 (vector-transfected +/+) and 2E6 (H/N) determined by MTT assay, and Figure 4.4C illustrates the average SMD2485 IC_{50} from CV assay for clones A6 (vector-transfected +/+), 2E6 (H/N), 1C8 (N/N), 2H8 (N/N) and 1A9 (H/H). The SMD2485 IC_{50} for clones A6 and 2E6 from the CV assay was close to the IC_{50} determined by MTT assay, suggesting that MTT assay is a reliable method to measure sensitivity to SMD2485 in OV90 cells. The overall average IC_{50} from both MTT and CV assays for all selected OV90 clones, parental OV90 cells and UWB1.289 cells are illustrated in Figure 4.4B. No statistical analysis was done on clones 2H8, 1A9 and parental OV90 cells because their drug-sensitivity tests were conducted in two biological repeats and the comparison to other cell lines might not be reliable. There is no statistical difference in the IC_{50} of SMD2485 between the vector-transfected clone A6 (+/+) and clones 2E6 (H/N) and 1C8 (N/N) that had different edited *BRCA1* alleles. The IC_{50} for vector-

transfected clone A6 (3.05μM) is significantly higher than the IC_{50} for UWB1.289 cells (0.722μM) and a p-value of 0.0037 between the two IC_{50} shows that the difference is significant.

Although the MTT assay and the CV assay allow for a rapid evaluation of the FEN1-inhibitor-sensitivity in OV90 clones, the use of such assays to measure metabolism or viable cell number immediately after the 3-day drug treatment may not accurately reflect the response of OV90 cells to SMD2485 in the long term. Given that there may be a latent period between drug exposure and cell death, I used clonogenic assay as a third method to assess the long-term effects of SMD2485 on the survival and proliferation of cells. Because clonogenic assay requires more time and materials to complete, only clones A6 (vector-transfected), 2E6 (H/N) and 1C8 (N/N) were chosen for the experiments. Cells were treated with 60μM, 20μM, 6μM, 2μM, 0.6μM, 0.2μM SMD2485 or DMSO or left untreated for 3 days and allowed to grow in fresh media for the next 3 days, and the resulting colonies were fixed, stained, imaged and counted (Figure 4.5A). Cells of clones A6, 2E6, 1C8 treated with 60μM, 20μM or 6μM of SMD2485 appeared to form no colonies. Substantial numbers of colonies were observed in the untreated cells, DMSO-treated cells as well as cells treated with 0.6μM or 0.2μM of SMD2485 for all three selective clones. Cells of the three clones treated with 2μM of SMD2485 formed colonies, but at an extent much less than that observed in cells treated with lower drug concentrations. The sizes of colonies formed are similar among clones A6, 2E6 and 1C8 across all treatment conditions (Figure 4.5B). The numbers of colonies counted by Fiji in clones A6, 2E6 and 1C8 following treatment of different SMD2485 concentrations are summarized in Figure 4.5C. Cells of clones A6, 2E6 and 1C8 formed only a few colonies at 6μM of SMD2485 or higher and started to form an average of 150 colonies at 2μM of SMD2485, indicating 2μM is close to the threshold beyond which OV90 cells are hard to recover from drug exposure. There is no significant

difference in the number of colonies formed by cells treated with 0.6μM or 0.2μM SMD2485. DMSO appears to have negligible effects on the ability of OV90 cells to form colonies as the number of colonies formed by DMSO-treated cells does not differ significantly from the untreated cells for all three clones. The IC_{50} of SMD2485 for clones A6, 2E6 and 1C8 determined by clonogenic assay are summarized in Table 4.2. There is no difference in the SMD2485 IC_{50} between clone 1C8 (N/N) and clones A6 (vector-transfected) and 2E6 (H/N), and the IC_{50} for the three OV90 clones is about 4.5 times higher than that for UWB1.289 cells.

The results from both short-term MTT/CV assay and long-term clonogenic assay show that the two OV90 clones 1C8 and 2H8, which contained only null alleles (N/N), were not sensitive to FEN1-inhibitor SMD2485, suggesting that BRCA1-editing did not lead to FEN1-inhibitor-sensitivity. Given that the two *BRCA1*-null alleles, one with a 52-nucleotide deletion and the other with a 40-nucleotide deletion, were predicted to produce BRCA1 amino acid sequences with length of 784 amino acids and 775 amino acids, respectively (Figure 4.3C), it was possible that the null alleles could make a truncated BRCA1 protein that retained the function sufficient to make the *BRCA1*-null cells not sensitive to SMD2485. Therefore, analysis of the BRCA1 protein in OV90 clones 1C8 and 2H8 was needed to confirm that the two clones were *BRCA1*-null and the in-sensitivity to FEN1-inhibitor SMD2485 was due to the truncated BRCA1 protein produced by the null alleles.

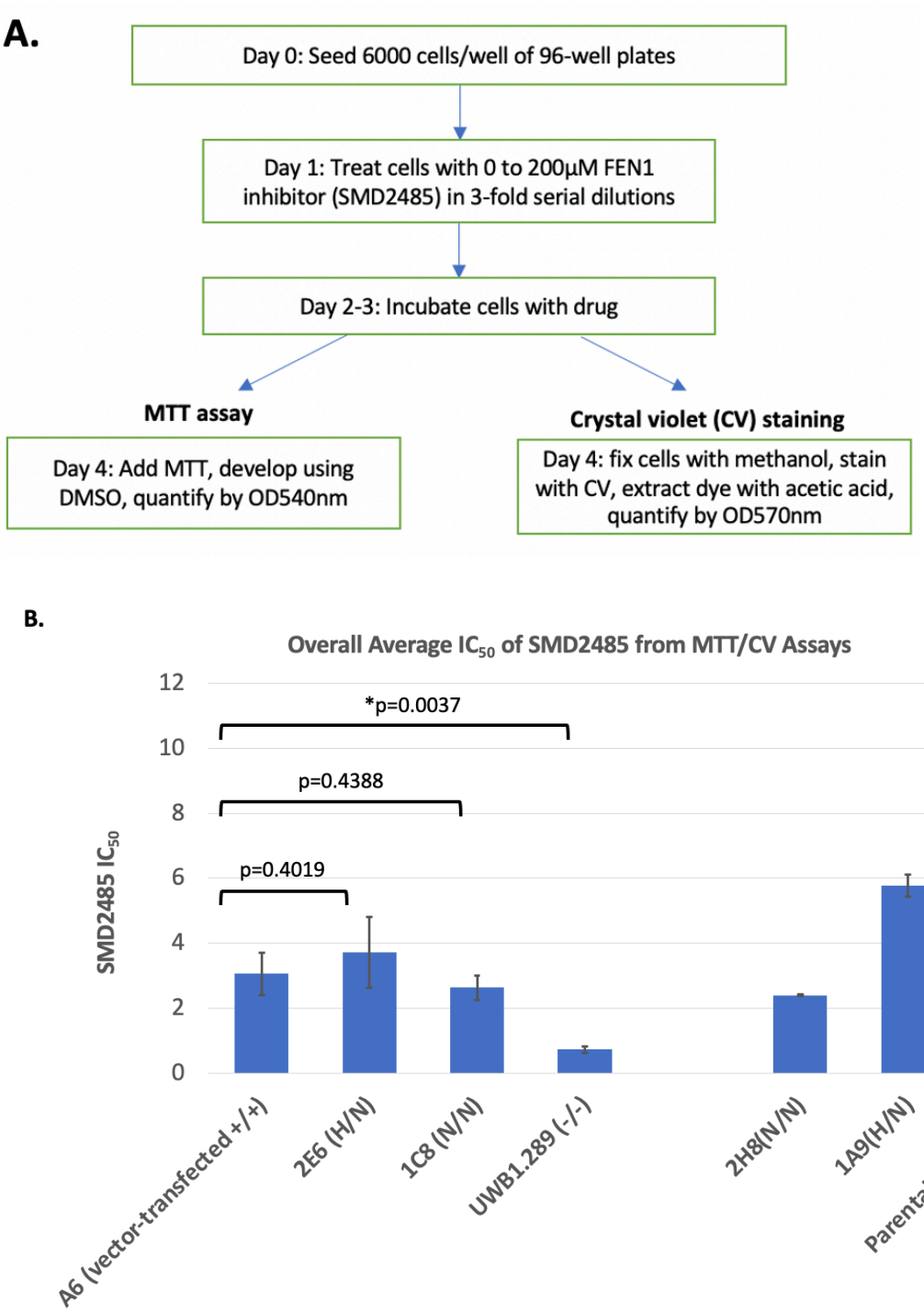

Figure 4. 4 Sensitivity to FEN1 inhibitor (SMD2485) in selected OV90 clones after 3-day drug treatment. (A) Experimental flow chart for measuring the SMD2485 IC_{50} values. (B) SMD2485 IC_{50} values for OV90 clones, parental OV90 cells and UWB1.289 cells from MTT assay and CV assay following three-day of drug treatment. Values shown are mean and standard deviations. p-values from *t*-test are shown above the square brackets.

C.

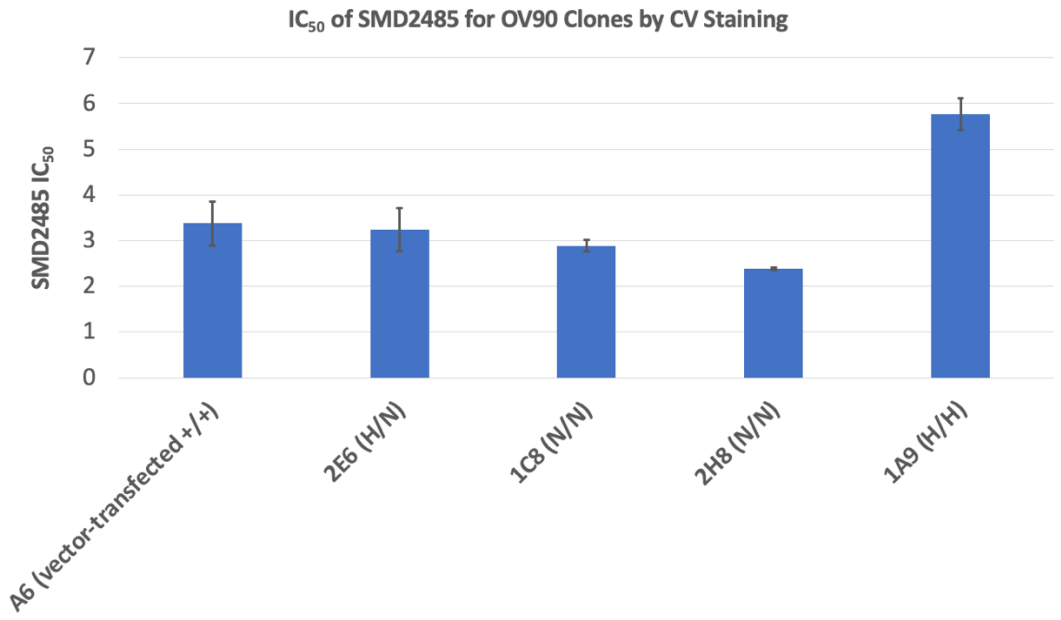

D.

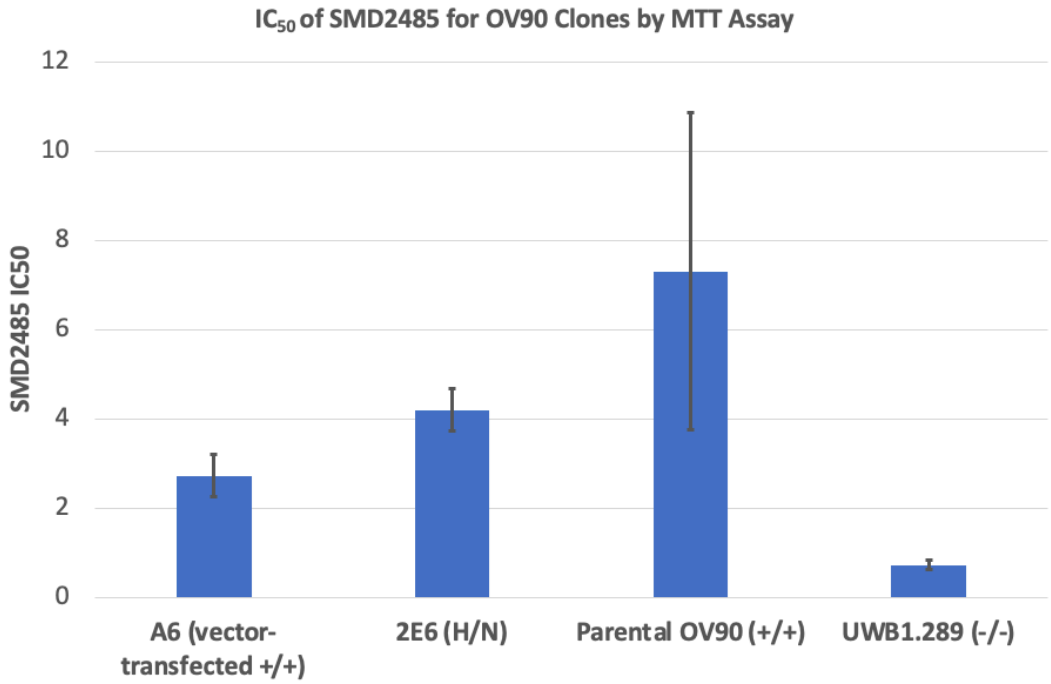

Figure 4.4 Sensitivity to FEN1 inhibitor (SMD2485) in selected OV90 clones after 3-day drug treatment, Continued. (C) SMD2485 IC_{50} values for selected OV90 clones (A6, 2E6, 1C8, 2H8, 1A9) from CV assay. (D) SMD2485 IC_{50} values for selected OV90 clones (A6, 2E6) from MTT assay.

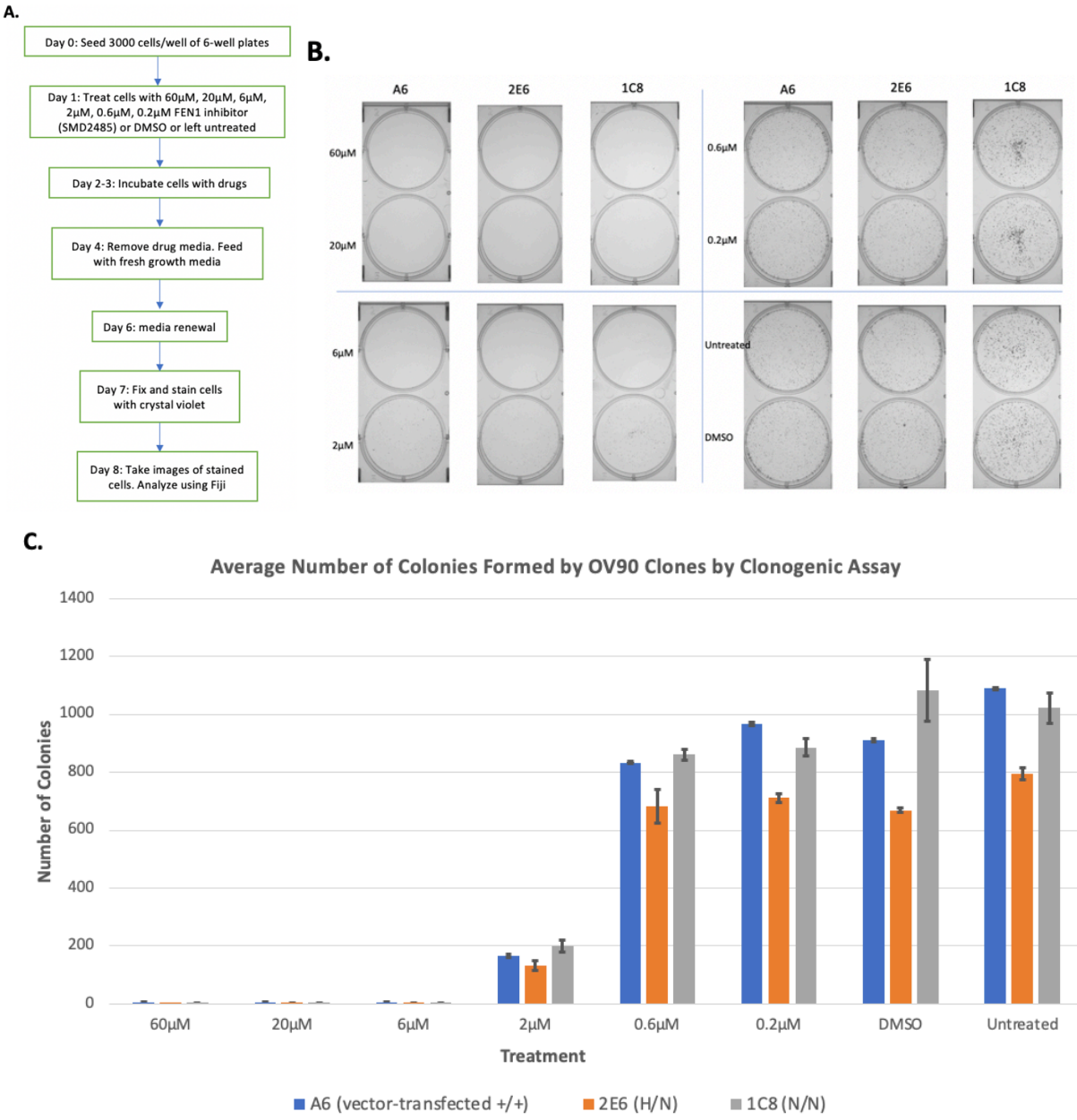

Figure 4.5 Sensitivity to FEN1 inhibitor (SMD2485) in selected OV90 clones by clonogenic assay. (A) Experimental flow chart for SMD2485 clonogenic assay. (B) Representative images of the clonogenic assay of selected OV90 clones. (C) Number of colonies in each of the indicated clones following treatment with the indicated concentrations of SMD2485. Values shown are average and standard deviation of colony numbers from three technical repeats per sample.

Table 4.2 IC_{50} of SMD2485 for selective OV90 clones determined by clonogenic assay.

Cell Lines	IC_{50} (μM) by clonogenic assay
A6 (vector-transfected +/+)	1.03
2E6 (H/N)	1.21
1C8 (N/N)	1.26
UWB1.289 (-/-)	0.25

4.2.5 BRCA1 Protein Analysis in OV90 Clones

To assess the BRCA1 protein level in OV90 clones, cells of the vector-transfected clone A6, and sgRNA-transfected clones 2E6 (H/N), 1C8 (N/N), 1A9 (H/H) and 2H8 (N/N) were collected and lysed and the protein extracts were analyzed by western blot using a BRCA1 antibody and a GAPDH antibody (loading control). The cells collected for blotting had been passaged 6 times for clones 2E6, 2H8 and 1A9, 7 times for vector-transfected clone A6 and 9 times for clone 1C8 since the day when the sequences of edited *BRCA1* alleles were first obtained (Figure 4.6A). The anti-GAPDH blot shows that the GAPDH protein bands with the expected MW of 37 kDa are detected in all samples at approximately the same intensity, indicating that about equal amounts of proteins were loaded and transferred across all wells of the western blot (Figure 4.6B). Parental OV90 cells used as a positive control demonstrates the banding patterns of wild-type BRCA1 protein on the Western blot. A protein band with the expected MW of 220 kDa as well as two bands with a higher and a lower size than the expected MW were detected in the *BRCA1*-wt parental OV90 cells, but not the *BRCA1*-null UWB1.289 cells (Figure 4.6B). The anti-BRCA1 blot shows that the BRCA1 protein bands observed in parental OV90 cells are also present in all selected OV90 clones, irrespective of the allele designations. In other words, the BRCA1 protein was detected in clones 1C8 and 2H8 that contain only *BRCA1*-null alleles based on sequencing (Figure 4.3). The protein analysis results show that clones 1C8 and 2H8 were not *BRCA1*-null as they expressed BRCA1 proteins with wild-type size. One possible explanation for the detection of BRCA1 protein bands in clones 1C8 and 2H8 is that these cultures became contaminated with *BRCA1*-wild type cells during propagation of the clones. The second possibility is that clones 1C8 and 2H8 were *BRCA1*-null

when first sequenced but their null-alleles reverted to hypomorphic ones to encode BRCA1 protein with small in-frame deletions during the 6-9 passages.

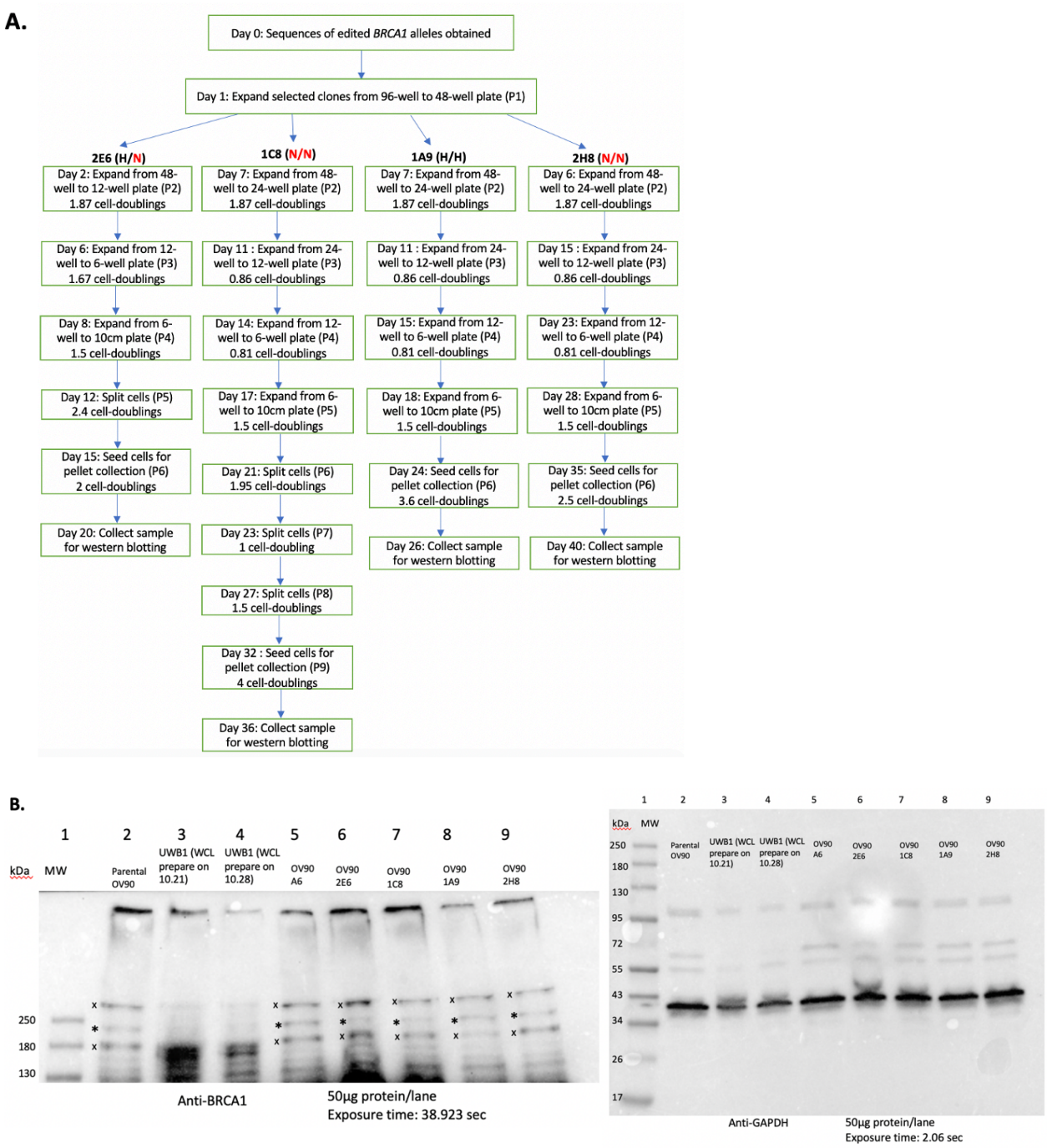

Figure 4.6 Analysis of BRCA1 protein in OV90 clones. (A) Experimental timeline for expansion of OV90 clones for analysis of BRCA1 protein. (B) Whole cell lysates were probed with anti-BRCA1 and anti-GAPDH. Parental OV90 cells (lane 1) were used as a positive control and the *BRCA1*-null UWB1.289 cells (lane 2,3) were used as a negative control. The BRCA1 protein band with the expected MW of 220 kDa detected in lane 1 but not in lanes 2 and 3 is marked by *. Two other protein bands with a higher and a lower size than the expected MW are also detected in lane 1 but not in lanes 2 and 3 and they are marked by x. The loading control GAPDH protein bands with the expected MW of 37kDa were detected in all samples.

4.2.6 Frame-Shift Reversions of *BRCA1*-Null Alleles

To determine whether the detection of BRCA1 protein bands in clones 1C8 and 2H8 is due to contamination with *BRCA1*-wild type cells or conversion of null-alleles to hypomorphic-alleles, I extracted the genomic DNA from clone 1C8 at passage 10 and clone 2H8 at passage 7 and re-analyzed the sequences of their edited *BRCA1* alleles. If *BRCA1*-wt cells were to have contaminated the cultures of clones 1C8 and 2H8, I would expect the detection of wild-type *BRCA1* and the original edited null-allele sequences. As summarized in Figure 4.7A, the sequence analyses did not detect any wild-type *BRCA1* sequences from either clone. At passage 10, clone 1C8 retained the original null allele but acquired three additional alleles. Two of the newly acquired alleles retained the original 51-nucleotide deletion but acquired an insertion of T at the sgRNA209 cut site (position 43,093,208 of chromosome 17, GRCh38), whereas another retained the original 48-nucleotide deletion but had a 3-nucleotide insertion at position 43,093,157 in addition to the insertion of T at 43,093,208. Besides small insertions, one of the newly acquired alleles had a G to A transversion mutation at position 43,093,098 and another had a T to G transversion mutation at position 43,093,096. At passage 7, clone 2H8 retained one of the original two null alleles and acquired a modified allele that differed from the other original null allele by a 6-nucleotide deletion at position 43,093,151 and a 7-nucleotide insertion at position 43,093,186. These results showed that the cultures were not contaminated with *BRCA1*-wt cells.

For each of the newly acquired *BRCA1* alleles in clones 1C8 and 2H8, the sequence alterations restored the wild-type *BRCA1* reading frame (Figure 4.7B), which was likely to account for the detection of BRCA1 protein by immunoblotting (Figure 4.7B). In clone 1C8, the two *BRCA1* alleles that retained the 51-nucleotide deletion of the original null allele and acquired

a T-insertion was predicted to result in a 17-amino acid in-frame deletion in the wild-type BRCA1 protein sequence, whereas another allele that retained the original 48-nucleotide deletion and had a 3-nucleotide insertion in addition to the T-insertion was predicted to generate BRCA1 protein with a 16-amino acid in-frame deletion. In clone 2H8, the modified allele was predicted to result in a 17-amino acid in-frame deletion. The results showed that the original null-alleles in clones 1C8 and 2H8 reverted to hypomorphic alleles as the cells were passaged in culture. Clone 1C8 after 10 passages had the *BRCA1*-genotype as H/H/H/N, and clone 2H8 after 7 passages had the genotype of H/N (Table 4.3).

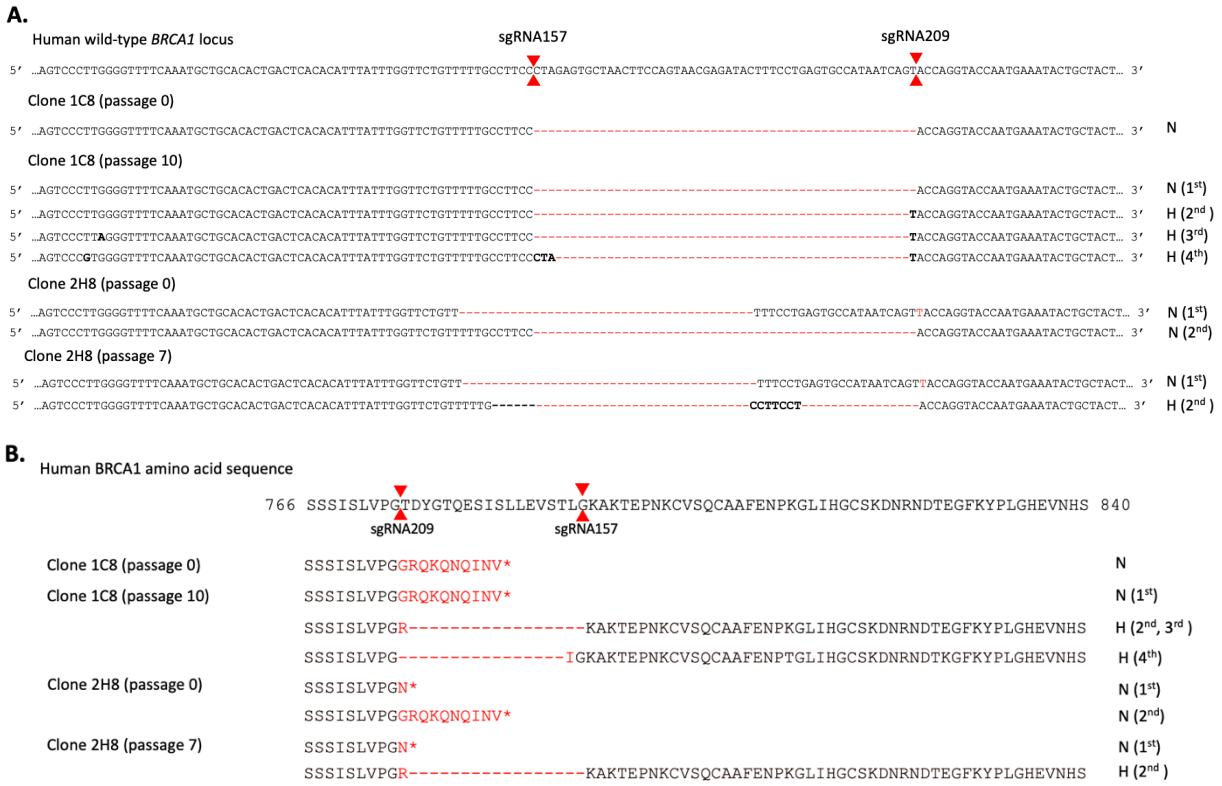

Figure 4.7 Frame-shift reversions of *BRCA1-null* alleles. (A) Nucleotide sequences of genomic PCR products from OV90 1C8 and 2H8 clones after 7-10 passages. Clone 1C8 retains the original null allele but acquires three additional alleles with insertions and single base substitutions indicated in bold letters. Clone 2H8 retains one of the original two null alleles but acquires an allele with insertions and deletions indicated in bold letters. (B) Predicted amino acids from the *BRCA1* sequences in clones 1C8 and 2H8 after 7-10 passages. Altered amino acids in red letters and missing amino acids are represented by red dashed lines. After 7-10 passages, clones 1C8 and 2H8 contained *BRCA1*-alleles that have undergone frame-shift reversions to generate BRCA1 proteins with small in-frame deletions.

Table 4.3 Summary of the analyses of edited BRCA1 alleles in OV90 1C8 and 2H8 clones before passages and after 7-10 passages.

Clone	Days & Passage Number	Number of TOPO-clones sequenced	Number of clones containing the expected PCR products	Number of alleles	Nature of Mutations Hypomorph (H): small in-frame deletion Null (N): premature termination
1C8	Day 0 (P0)	7	7	1	N/N
	Day 34 (P10)	8	7	4	H/H/H/N
2H8	Day 0 (P0)	6	2	2	N^1/N^2
	Day 40 (P7)	8	4	2	H/N^1

4.3 References

Bothmer, A., Phadke, T., Barrera, L. A., Margulies, C. M., Lee, C. S., Buquicchio, F., Moss, S., Abdulkerim, H. S., Selleck, W., Jayaram, H., Myer, V. E., & Cotta-Ramusino, C. (2017). Characterization of the interplay between DNA repair and CRISPR/Cas9-induced DNA lesions at an endogenous locus. *Nature communications*, *8*, 13905. https://doi.org/10.1038/ncomms13905

Cong, L., Ran, F. A., Cox, D., Lin, S., Barretto, R., Habib, N., Hsu, P. D., Wu, X., Jiang, W., Marraffini, L. A., & Zhang, F. (2013). Multiplex genome engineering using CRISPR/Cas systems. *Science (New York, N.Y.)*, *339*(6121), 819–823. https://doi.org/10.1126/science.1231143

Goodwin, E. C., & Rottman, F. M. (1992). The 3'-flanking sequence of the bovine growth hormone gene contains novel elements required for efficient and accurate polyadenylation. *The Journal of biological chemistry*, *267*(23), 16330–16334.

Gray, S. J., Foti, S. B., Schwartz, J. W., Bachaboina, L., Taylor-Blake, B., Coleman, J., Ehlers, M. D., Zylka, M. J., McCown, T. J., & Samulski, R. J. (2011). Optimizing promoters for recombinant adeno-associated virus-mediated gene expression in the peripheral and central nervous system using self-complementary vectors. *Human gene therapy*, *22*(9), 1143–1153. https://doi.org/10.1089/hum.2010.245

Guo, E., Ishii, Y., Mueller, J., Srivatsan., A., Gahman, T., Putnam, C.D., Wang, J., & Kolodner, R.D. (2020). FEN1 endonucleases as a therapeutic target for human cancers with defects in homologous recombination. *Proceedings of the National Academy of Sciences*, 117(32), 19415-19424. doi: 10.1073/pnas.2009237117

Hongo, T., Mizuno, Y., Haraguchi, S., & Yoshida, T. O. (1986). *Gan to kagaku ryoho. Cancer & chemotherapy*, *13*(2), 247–254.

Liu, Z., Chen, O., Wall, J.B.J., Zheng, M., Zhou, Y., Wang, L., Vaseghi, H., Qian, L., & Liu, J. (2017). Systematic comparison of 2A peptides for cloning multi-genes in a polycistronic vector. *Sci Rep,* 7(2193). https://doi.org/10.1038/s41598-017-02460-2

Perrin-Vidoz, L., Sinilnikova, O. M., Stoppa-Lyonnet, D., Lenoir, G. M., & Mazoyer, S. (2002). The nonsense-mediated mRNA decay pathway triggers degradation of most BRCA1 mRNAs bearing premature termination codons. *Human molecular genetics,* 11(23), 2805-2814. https://doi.org/10.1093/hmg/11.23.2805

Ran, F. A., Hsu, P. D., Wright, J., Agarwala, V., Scott, D. A., & Zhang, F. (2013). Genome engineering using the CRISPR-Cas9 system. *Nature protocols*, *8*(11), 2281–2308. https://doi.org/10.1038/nprot.2013.143

Tate, J. G., Bamford, S., Jubb, H. C., Sondka, Z., Beare, D. M., Bindal, N., Boutselakis, H., Cole, C. G., Creatore, C., Dawson, E., Fish, P., Harsha, B., Hathaway, C., Jupe, S. C., Kok, C. Y., Noble, K., Ponting, L., Ramshaw, C., Rye, C. E., Speedy, H. E., Stefancsik, R., Thompson, S. L., Wang, S., Ward, S., Campbell, P. J., Forbes, S. A. (2019). COSMIC: the Catalogue Of Somatic

Mutations In Cancer. *Nucleic Acids Research*, 47(D1), 941-947. https://doi.org/10.1093/nar/gky1015

van Meerloo, J., Kaspers, G. J., & Cloos, J. (2011). Cell sensitivity assays: the MTT assay. *Methods in molecular biology (Clifton, N.J.)*, *731*, 237–245. https://doi.org/10.1007/978-1-61779-080-5_20

Zhang, L., Hernan, R. & Brizzard, B. (2001). Multiple tandem epitope tagging for enhanced detection of protein expressed in mammalian cells. *Mol Biotechnol*, 19, 313–321. https://doi.org/10.1385/MB:19:3:313

CHAPTER 5 DISCUSSION

5.1 Differential Sensitivity of OV90 and UWB1.289 Ovarian Cancer Cells to FEN1 Inhibitor

In this study, I measured the sensitivities of OV90 cells with *BRCA1*-wt or hypomorphic alleles and *BRCA1*-null UWB1.289 cells to SMD2485, a FEN1 inhibitor that was not tested in the previous study (Guo et al., 2020), by three different assays, namely the short-term MTT and CV assays and the longer-term colony forming assay. The results I obtained are consistent with previous results obtained with SMD154 and *FEN1*-siRNA in that the IC_{50} value of SMD2485 for the BRCA1-proficient OV90 ovarian cancer cells is about 4 times higher than that of the BRCA1-deficient UWB1.289 ovarian cancer cells (Figure 4.4B and Table 4.2). I found that the IC_{50} determined by clonogenic assay is much lower than that from the MTT and CV assays, suggesting that the longer-term effect of SMD2485 on cell proliferation is more severe than its immediate effect on cell metabolic activity (measured by MTT reduction) or total cellular proteins (measured by CV staining). In addition, I found that the SMD2485 IC_{50} for a vector-transfected OV90 clone did not differ significantly from that for OV90 clones with hypomorphic *BRCA1* alleles encoding BRCA1 with small in-frame deletions in Exon-10 (Figure 4.4B), showing that those BRCA1 proteins with internal truncations were as resistant to SMD2485 as the *BRCA1*-wt OV90 cells. Annotation of the Human BRCA1 protein shows that the amino acids deleted in the hypomorphic alleles of the OV90 clones are not located in key domains of BRCA1, and aligning the Human and the Mouse BRCA1 proteins sequences shows that the deleted amino acids are conserved at 62% level (Figure 5.1), suggesting that those relatively conserved amino acids are likely not important for BRCA1 to negate the requirement for FEN1, thereby providing an explanation for the resistance to SMD2485 in OV90 cells that express

BRCA1 protein with those deletions. This study failed to determine the effect of *BRCA1*-knockout on the response of OV90 cells to SMD2485 because the *BRCA1*-null alleles created by the CRISPR/Cas9 editing events rapidly reverted to hypomorphic alleles during propagation of those OV90 clones.

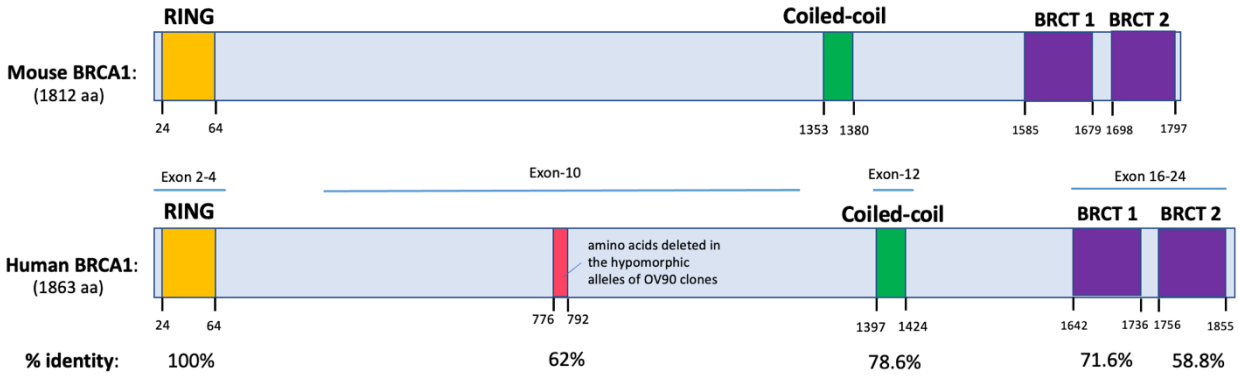

Figure 5.1 Amino Acid Conservation between Mouse and Human BRCA1. The RING (Really Interesting New Gene) domain is in yellow, the Coiled-coil domain is in green and the two tandem BRCT (BRCA1 C-terminal) domains are in purple. The region where amino acids were deleted in the hypomorphic alleles of the OV90 clones is in red. The exons that correspond to each domain of the Human BRCA1 and the percent identity between each domain of the human and mouse BRCA1 after alignment are shown.

5.2 Reversion of *BRCA1*-Null Alleles in OV90 Clones

The instability of the *BRCA1*-null alleles in OV90 clones was revealed by re-analysis of the edited *BRCA1*-sequences in OV90 clones 1C8 and 2H8 after 7-10 passages. The edited null-alleles with premature-termination codons appeared to have been further mutated to generate hypomorphic alleles that encode BRCA1 proteins with small in-frame deletions (Figure 4.7). The reversions of the two *BRCA1*-null alleles in clone 1C8 were from either a 1-nucleotide insertion or a 4-nucleotide insertion in the original null alleles, whereas the reversion of the single *BRCA1*-null allele in clone 2H8 involved a 7-nucleotide insertion plus a 6-nucleotide deletion in the original null allele (Figure 4.7A). Reversion of mutant *BRCA1* in ovarian cancer cells has previously been observed in a study that characterized *BRCA1* and *BRCA2 (BRCA1/2)* status in 41 ovarian cancer cell lines derived from 33 different ovarian cancer patients (Stordal et al., 2013). With the UPN-251 ovarian cancer cell line, which possessed a homozygous deletion of 29 nucleotides in exon-11 of *BRCA1* causing a premature stop codon, reversion was observed by a single nucleotide deletion located 47 bp downstream of the 29-nucleotide deleterious mutation to restore the wild-type *BRCA1* reading frame (Stordal et al., 2013). In the review article that summarized *BRCA1/2* secondary mutations in both cancer cell line models and clinical samples of ovarian cancer, Dhillon et al. (2011) found that reversion mutations often involved small insertions and deletions. It thus appears that small insertions and deletions are a common way by which *BRCA1*-null alleles can revert to hypomorphic alleles to produce BRCA1 proteins with small in-frame deletions. The instability of *BRCA1*-null alleles in ovarian cancer cell lines, including the OV90 clones generated from this study, is likely due to two factors: (1) loss of BRCA1 increases the rate of insertion and deletion mutations (Zámborszky et al., 2017) and (2) loss of BRCA1 comprises DNA replication and repair to reduce cell fitness.

Mechanisms that generate small insertion and deletion mutations include polymerase slippage, imperfect repair of double-stranded breaks (DSBs), defective mismatch repair and unequal crossover (Sehn, 2015). Given that *BRCA1*-defective cells have impaired homologous recombination (HR) and need to rely on the error-prone non-homologous end joining (NHEJ) to repair the DSBs (Rosen, 2013; Tarsounas & Sung, 2020), small insertion and deletion mutations are more likely to occur in *BRCA1*-defective cells. It has been shown that loss of BRCA1 increases the rate of spontaneous arising insertion mutations by 2-fold and deletion mutations by 8-fold in *BRCA1*-mutant cells relative to wild-type cells (Zámborszky et al., 2017). Therefore, it is unsurprising to find in this study that the edited *BRCA1*-null alleles rapidly acquired insertion and deletion mutations to restore protein expression.

Besides the higher mutation rate, the growth disadvantage of *BRCA1*-nulls cells is likely to have also driven the reversion of null mutations. BRCA1-deficiency leads to impaired DNA damage response, growth retardation, defective cell cycle checkpoint as well as increased apoptosis (Deng, 2006). It is rare to observe and difficult to develop cell lines with complete loss of BRCA1 in cell culture. Out of the 41 ovarian cancer cell lines studied by Stordal et al. (2013), only one cell line (SNU-251), which was established with difficulty in cell culture, has a homozygous deleterious *BRCA1* mutation that results in a frameshift and premature termination. Of the 12 OV90 clones I created, 7 had one hypomorphic allele and one null allele (H/N), 3 had two hypomorphic alleles (H/H) and 2 had only null alleles (N/N) (Table 4.1). The observation that the majority of clones (10/12) had at least one *BRCA1* allele with small in-frame internal deletion that could produce a nearly full-length protein showed that *BRCA1*-null single cells were less likely to proliferate into clones. The observation that the two *BRCA1*-null clones (1C8 and 2H8) lost their null-alleles within 10 passages in culture further demonstrates the growth

disadvantage of *BRCA1*-deficient OV90 cells. Since the literature and my experimental observations both show that there is a strong selection for BRCA1-function for cell line propagation, it can be concluded that *BRCA1*-proficient cells must have a growth advantage over *BRCA1*-null cells. As a result, during the expansion of *BRCA1*-null OV90 clones, the higher rate of mutation combined with the increased fitness of hypomorphic revertants caused the loss of *BRCA1*-null cells.

In the clinic, reversion of *BRCA1*/*2*-mutant cancer cells have emerged as a mechanism of acquired resistance to platinum-based chemotherapy and to PARP inhibitors (Dhillon et al., 2011; Stordal et al., 2013). Given that the reversion mutations observed in the two OV90 clones (1C8 and 2H8) rapidly emerged during passaging of the cells without any selective pressure, we cannot rule out the possibility that the hypomorphic alleles observed in the re-analysis of edited *BRCA1*-sequences in clones 1C8 and 2H8 might have been pre-existing in the cell population at a frequency too low to be detected by the initial sequence analysis. These hypomorphic alleles became the dominant ones after 10 passages because they conferred a growth advantage over cells that only possessed the null alleles. Hence, we cannot rule out the possibility that the 1C8 and the 2H8 populations were not derived from a single cell and that a cell with the hypomorphic allele was present from the beginning of the clonal isolation process.

5.3 Stability of *BRCA1*-null Allele in UWB1.289 Cells

In contrast to the observed rapid reversion of *BRCA1*-null alleles in OV90 clones, UWB1.289 ovarian cancer cells have remained BRCA1-null despite propagation as a cell line in culture for 13 years (Dellorusso et al., 2007) and in our cell culture experiments. As discussed above, *BRCA1*-null cells have higher mutation rates that drive genome instability and cancer development (Rosen, 2013; Tarsounas & Sung, 2020), and *BRCA1*-null alleles can readily undergo reversion mutations to produce functional BRCA1 protein (Dhillon et al., 2011; Stordal et al., 2013). However, the higher mutation rate does not appear to drive the reversion of the single nucleotide deletion in exon-10 found in UWB1.289 cells. Since there is a strong selection for BRCA1-function during cell line propagation, I find the stability of the *BRCA1*-null alleles in UWB1.289 cells to be interesting. I can envision two possibilities for how the *BRCA1*-null allele might be maintained in UWB1.289 cells. The first being an adaptation that allows UWB1.289 cells to gain fitness despite the loss of BRCA1, and the second being the specialized media used to propagate UWB1.289 cells.

It is also possible that in the context of UWB1.289 cells, certain genetic and epigenetic adaptations have been selected for during tumor development such that BRCA1-loss no longer affects cell growth, or that restoration of BRCA1 function may even have deleterious effects and is therefore not selected-for during cell line propagation. In the initial characterization of the function of the *BRCA1* gene in the 1990s, Thompson and her colleagues (1995) found that sporadic invasive breast cancer expressed *BRCA1* at 4 to 8 times higher levels than non-invasive breast cancer. By inhibiting BRCA1 expression using antisense oligonucleotides in primary mammary epithelial cells and MCF-7 breast cancer cells, Thompson et al. (1995) found that both normal and breast cancer cells treated with anti-BRCA1 oligonucleotides showed faster

proliferate rate. In other studies, retroviral transfer of the wild-type, but not mutant, *BRCA1* gene into breast cancer cell lines (MCF-7 and MDA-MB-157) and ovarian cancer cell lines (Caov-4, ES-2 and PA-1) was shown to significantly inhibited cell growth (Holt et al., 1996). Thus, it is conceivable that wild-type *BRCA1* might exert a growth inhibitory effect in UWB1.289 ovarian cancer cells such that that *BRCA1*-null mutation might be more advantageous to cell growth. In the previous study where UWB1.289 cell line was first developed, a *BRCA1*-wt derivative (UWB1.289+BRCA1) was also generated by stable transfection with a pcDNA3 plasmid carrying wild-type *BRCA1* and was shown to stably integrated the pcDNA3-BRCA1 plasmid into the genome and express high level of wild-type BRCA1 protein (Dellorusso et al., 2007). Experiments conducted in that study showed that UWB1.289+BRCA1 cells had a growth rate not significantly differ from that of UWB1.289 cells and showed partially restored S and G_2-M phase DNA damage checkpoints following ionizing radiation exposure (Dellorusso et al., 2007). The observations that wild-type *BRCA1* did not suppress growth and the restoration of BRCA1-function partly restored DNA damage responses in UWB1.289 cells refute the hypothesis that BRCA1 function had a deleterious effect on UWB1.289 cells. However, it cannot be ruled out that UWB1.289 cells could have gained functions to neutralize the DNA replication and/or repair defects associated with BRCA1-loss such that BRCA1-loss no longer affects the growth of UWB1.289 cells.

Besides cell-intrinsic adaptations, the stability of *BRCA1*-null allele in UWB1.289 cells may also be due to cell-extrinsic factors. To culture UWB1.289 cells, I used serum-free Mammary Epithelial Cell Basal Medium (MEBM) and Roswell Park Memorial Institute (RPMI)-1640 Medium with the following supplements: bovine pituitary extract (BPE), human epidermal growth factor (hEGF), insulin and hydrocortisone (HC). BPE contains a variety of

growth factors including growth hormone (GH), fibroblast growth factor (FGF), platelet-derived growth factor, luteinizing hormone (LH), follicle stimulating hormone (FSH) and human chorionic gonadotropin (hCG) that stimulate the proliferation of ovarian epithelial cells (Kent & Bomser, 2003; Kuroda et al., 2001; Li et al., 2004). Besides the mitogenic effects of the growth factors in BPE, BPE also protects cells against oxidative stress (Kent & Bomser, 2003). hCG in BPE has been shown to significantly reduce apoptosis induced by nutrient deprivation in ovarian surface epithelial (OSE) cells (Kuroda et al., 2001). Exogenous hEGF ensures the constitutive activation of EGF receptor (EGFR) in ovarian cancer cell lines, thereby activating the EGFR cell proliferation signaling pathways that promote cell growth and drive cell cycle progression (Ottensmeier et al., 1996; Wee & Wang, 2017). Insulin acts as a growth factor *in vitro* and interacts synergistically with other growth factors, such as EGF and platelet-derived growth factor, to induce the progression from G1 to S phase (Hill & Milner, 1985), whereas HC enhances the mitogenic effect of hormonal growth factors including EGF and insulin on cells (Hoshi et al., 1982). OSE cells, cultured in medium supplemented with a combination of BPE, EGF, insulin and HC, had significantly higher cloning efficiency and faster population doublings than cells in non-supplemented medium (Li et al., 2004). Therefore, it is possible that the growth factors present in the culture media alleviate the negative impacts of BRCA1-loss on UWB1.289 cells and support cell fitness in culture. One way to test whether the highly enriched media allows UWB1.289 cells to grow without BRCA1 would be to culture UWB1.289 cells in non-supplemented media or in media supplemented with BPE, EGF, HC and insulin individually or in combinations, and then sequence the *BRCA1* alleles after 10 passages. If one or more growth factors in the supplements were required for UWB1.289 cells to grow without BRCA1, we would expect to detect reversion of the *BRCA1*-null allele in UWB1.289 cells following

propagation in media lacking such growth factors. However, removal of the supplements may hinder the propagation of UWB1.289 cells all together and it may not be possible to carry out 10 passages of UWB1.289 cells in supplement-free media before the sequence analysis. An alternative way to test the idea that one or more growth factors in the supplements may stabilize the *BRCA1*-null allele would be to repeat the cloning and propagation of edited OV90 cells in media containing the supplements, and determine whether the supplements would increase the frequency and stability of *BRCA1*-null alleles among OV90 clones following CRISPR/Cas9-editing.

5.4 Alternative Strategies for Future Studies

Given the observations that *BRCA1*-null alleles created by nonsense mutations rapidly underwent reversion mutations to produce BRCA1 proteins with small in-frame deletions during propagation of the OV90 clones, the editing strategy I used in this study is not adequate to create stable *BRCA1*-null clones in OV90 cells. Alternative strategies to generate stable *BRCA1*-null OV90 cells are therefore needed to achieve this goal. The first alternative I can envision is to edit the highly conserved exons-2 to exon-4 (the RING domain) and exon-12 (the Coiled-coil domain) (Figure 5.1) of the *BRCA1* gene simultaneously so as to minimize the probability of restoring a functional BRCA1 protein. If the media supplements used to propagate UWB1.289 cells are indeed responsible for maintaining the *BRCA1*-null allele, I can also add those supplements to stabilize the edited *BRCA1*-null alleles during the cloning and propagation of *BRCA1*-null OV90 cells. The second alternative is to inducibly knock-out *BRCA1* in OV90 cells such that the effect of BRCA1-loss can be investigated without the need to propagate *BRCA1*-null OV90 clones.

The first alternative involves the introduction of multiple sgRNAs with different guide sequences to simultaneously target key exons of *BRCA1*, generating null mutations in multiple places of the *BRCA1* coding region. Although *BRCA1*-null alleles can undergo reversion mutations, it is less likely that the null mutations present in different locations of the *BRCA1* gene will revert concertedly to restore the wild-type *BRCA1* reading frame. Therefore, targeting multiple exons of the *BRCA1* gene with multiple sgRNAs might make it difficult for *BRCA1*-null alleles to revert to hypomorphic ones and thus increase the likelihood of generating stable *BRCA1*-null OV90 clones. The CRISPR/Cas9 system can be readily engineered for multiplexed targeting by co-expressing multiple sgRNA in cells through the delivery of single plasmids

carrying a CRISPR RNA array, a multi-sgRNA expression cassette, or an artificial multi-sgRNA precursor (Cao et al., 2016; Cao et al., 2018; McCarty et al., 2020). Several cloning methods have been developed to simplify the construction of multiple-sgRNA delivery plasmids, such as Gibson and Golden Gate Assembly (Cao et al., 2016; Cao et al., 2018; McCarty et al., 2020). Cao and his colleagues have shown that a one-step cloning strategy they designed based on the Golden Gate Assembly is effective in generating a single delivery plasmid containing up to six sgRNAs (Cao et al., 2016). Despite the advantages of using multiple sgRNAs to target multiple exons of *BRCA1* and the recent technical improvement in multiplexed CRISPR technologies, several challenges remain. It's more time- and effort-consuming to screen for clones with edited *BRCA1* alleles as multiple places in the *BRCA1* gene are targeted. With an increased number of sgRNAs, the off-target effects are more significant (Cao et al., 2018). Another obstacle for scaling the number of sgRNAs is the increased competition for Cas9 enzymes. It has been shown that sgRNA targeting efficiency drops as the number of sgRNAs expressed increases (Sun et al., 2019). Therefore, careful consideration needs to be taken when selecting multiple sgRNAs for targeting *BRCA1* in this multiplexed approach in order to achieve lower off-target effects and higher targeting efficiency.

Circumventing the efforts required to isolate *BRCA1*-alleles with simultaneous editing in multiple exons is a second alternative strategy, which relies on an inducible CRISPR/Cas9 system to conditionally knockout *BRCA1* in OV90 cells, allowing for direct measurements of knockout phenotype without having to propagate *BRCA1*-null OV90 cells. An inducible CRISPR/Cas9 system enables tighter control of Cas9/sgRNA, resulting in greater precision and fewer off-target events (Cao et al., 2016; Zhang et al., 2019). The activity of Cas9/sgRNA can be controlled through various inducible methodologies, including the use of small molecules, light

irradiation and heat shock (Cao et al., 2016; Zhang et al., 2019). One of the most widely used drug-inducible CRISPR/Cas9 systems is the doxycycline (dox)-induced Tet system that relies on a dox-inducible promoter for the expression of *Cas9* (Zhang et al., 2019). Using this system, Cao et al. demonstrated successful gene silencing after dox induction in cells integrated stably with inducible-*Cas9* gene and sgRNAs (Cao et al., 2016). With this strategy, the immediate consequences of gene knockout can also be assessed following the induction of Cas9 expression without the need to select and expand stable clones for downstream analyses, such as protein expression and drug sensitivity, leaving almost no time for reversion mutations to occur to restore protein functionality. Despite the advantages provided by the inducible CRISPR/Cas9 system, several limitations are to be considered. The chemicals used for induction may have undesirable effects on the cell (Sun et al., 2019). The Tet system can be leaky, resulting in Cas9 expression in the absence of dox and undesired gene editing (Sun et al., 2019). The inducible strategy is also not suitable for studying the long-term effect of gene knockout because gene-knockout cells might be overtaken by wild-type cells present in the edited cell population over time. Without generating stable knockout clones that can be subjected to analysis at convenience, this approach requires induction each time before performing functional assay.

Given that lipofection- or nucleofection-transfected UWB1.289 cells could not be propagated after selection for antibiotic resistance, the CRISPR/Cas9 repair template approach did not succeed in correcting *BRCA1* mutation in UWB1.289 cells. As a result, alternative strategies are needed to express wild-type BRCA1 in UWB1.289 cells are needed. One alternative I can think of is to use retroviral vector carrying *BRCA1*-wt cDNA to introduce *BRCA1* into UWB1.289 cells. Unlike classical lipid transfection or electroporation, retroviral vector-mediated gene transfer allows permanent integration of the DNA into the host cell

genome and ensures stable expression of the gene product (Anson, 2004). This gene delivery system might overcome the problem presented by the CRISRP/Cas9 editing strategy because the plasmid DNA would not remain in the cytoplasm and cause cytotoxicity in UWB1.289 cells. However, it is possible that the retroviral DNA gets integrated into an unintended site within the host genome and disrupt the host's normal functional genes, resulting in mutations and oncogenesis (Anson, 2004).

As the alternatives each has its own advantages and disadvantages, it will be worthwhile to try all of them in order to express wild-type BRCA1 in UWB1.289 cells and to knock-out *BRCA1* in OV90 ovarian cancer cells. Being able to create *BRCA1*-wt UWB1.289 cells as well as *BRCA1*-null OV90 cells and to measure their sensitivities to FEN1-inhibitor SMD2485 is crucial in establishing a causative relationship between *BRCA1*-mutation and FEN1-inhibitor-sensitivity so as to prove a synthetic lethal interaction between BRCA1 and FEN1.

5.5 References

Anson D. S. (2004). The use of retroviral vectors for gene therapy-what are the risks? A review of retroviral pathogenesis and its relevance to retroviral vector-mediated gene delivery. *Genetic vaccines and therapy*, *2*(1), 9. https://doi.org/10.1186/1479-0556-2-9

Cao, J., Xiao, Q., & Yan, Q. (2018). The multiplexed CRISPR targeting platforms. *Drug discovery today. Technologies*, *28*, 53–61. https://doi.org/10.1016/j.ddtec.2018.01.001

Cao, J., Wu, L., Zhang, S. M., Lu, M., Cheung, W. K., Cai, W., Gale, M., Xu, Q., & Yan, Q. (2016). An easy and efficient inducible CRISPR/Cas9 platform with improved specificity for multiple gene targeting. *Nucleic acids research*, *44*(19), e149. https://doi.org/10.1093/nar/gkw660

Dellorusso, C., Welcsh, P. L., Wang, W., Garcia, R. L., King, M.-C., & Swisher, E. M. (2007). Functional Characterization of a Novel BRCA1-Null Ovarian Cancer Cell Line in Response to Ionizing Radiation. *Molecular Cancer Research*, *5*(1), 35–45. doi: 10.1158/1541-7786.mcr-06-0234

Deng, C. X. (2006). BRCA1: cell cycle checkpoint, genetic instability, DNA damage response and cancer evolution. *Nucleic acids research*, *34*(5), 1416–1426. https://doi.org/10.1093/nar/gkl010

Dhillon, K. K., Swisher, E. M., & Taniguchi, T. (2011). Secondary mutations of BRCA1/2 and drug resistance. *Cancer science*, *102*(4), 663–669. https://doi.org/10.1111/j.1349-7006.2010.01840.x

Guo, E., Ishii, Y., Mueller, J., Srivatsan., A., Gahman, T., Putnam, C.D., Wang, J., & Kolodner, R.D. (2020). FEN1 endonucleases as a therapeutic target for human cancers with defects in homologous recombination. Proceedings of the National Academy of Sciences, 117(32), 19415-19424. doi: 10.1073/pnas.2009237117

Hill, D. J., & Milner, R. D. (1985). Insulin as a growth factor. *Pediatric research*, *19*(9), 879–886. https://doi.org/10.1203/00006450-198509000-00001

Holt, J. T., Thompson, M. E., Szabo, C., Robinson-Benion, C., Arteaga, C. L., King, M. C., & Jensen, R. A. (1996). Growth retardation and tumour inhibition by BRCA1. *Nature genetics*, *12*(3), 298–302. https://doi.org/10.1038/ng0396-298

Hoshi, H., Kan, M., Minamoto, Y., & Yamane, I. (1982). Hydrocortisone potentiates cell proliferation and promotes cell spreading on tissue culture substrata of human diploid fibroblasts in a serum-free hormone-supplemented medium. *Biomedical Research, 3*(5), 546-552. doi:10.2220/biomedres.3.546

Kent, K. D., & Bomser, J. A. (2003). Bovine pituitary extract provides remarkable protection against oxidative stress in human prostate epithelial cells. *In vitro cellular & developmental biology. Animal*, *39*(8-9), 388–394. https://doi.org/10.1290/1543-706X(2003)039<0388:BPEPRP>2.0.CO;2

Kuroda, H., Mandai, M., Konishi, I., Tsuruta, Y., Kusakari, T., Kariya, M., & Fujii, S. (2001). Human ovarian surface epithelial (OSE) cells express LH/hCG receptors, and hCG inhibits apoptosis of OSE cells via up-regulation of insulin-like growth factor-1. *International journal of cancer*, *91*(3), 309–315. https://doi.org/10.1002/1097-0215(200002)9999:9999<::aid-ijc1060>3.0.co;2-0

Li, N. F., Wilbanks, G., Balkwill, F., Jacobs, I. J., Dafou, D., & Gayther, S. A. (2004). A modified medium that significantly improves the growth of human normal ovarian surface epithelial (OSE) cells in vitro. *Laboratory investigation; a journal of technical methods and pathology*, *84*(7), 923–931. https://doi.org/10.1038/labinvest.3700093

McCarty, N. S., Graham, A. E., Studená, L., & Ledesma-Amaro, R. (2020). Multiplexed CRISPR technologies for gene editing and transcriptional regulation. *Nature communications*, *11*(1), 1281. https://doi.org/10.1038/s41467-020-15053-x

Ottensmeier, C., Swanson, L., Strobel, T., Druker, B., Niloff, J., & Cannistra, S. A. (1996). Absence of constitutive EGF receptor activation in ovarian cancer cell lines. *British journal of cancer*, *74*(3), 446–452. https://doi.org/10.1038/bjc.1996.379

Rosen, E.M. (2013). BRCA1 in the DNA damage response and at telomeres. *Frontiers in genetics*, 4, 85. https://doi.org/10.3389/fgene.2013.00085

Sehn, J. K. (2015). Chapter 9 - Insertions and Deletions (Indels). In S. Kulkarni & J. Pfeifer (Eds.), *Clinical Genomics* (129-150). Academic Press. https://doi.org/10.1016/B978-0-12-404748-8.00009-5.

Stordal, B., Timms, K., Farrelly, A., Gallagher, D., Busschots, S., Renaud, M., Thery, J., Williams, D., Potter, J., Tran, T., Korpanty, G., Cremona, M., Carey, M., Li, J., Li, Y., Aslan, O., O'Leary, J. J., Mills, G. B., & Hennessy, B. T. (2013). BRCA1/2 mutation analysis in 41 ovarian cell lines reveals only one functionally deleterious BRCA1 mutation. *Molecular oncology*, *7*(3), 567–579. https://doi.org/10.1016/j.molonc.2012.12.007

Tarsounas, M., & Sung, P. (2020). The antitumorigenic roles of BRCA1–BARD1 in DNA repair and replication. *Nat Rev Mol Cell Biol*. https://doi.org/10.1038/s41580-020-0218-z

Thompson, M. E., Jensen, R. A., Obermiller, P. S., Page, D. L., & Holt, J. T. (1995). Decreased expression of BRCA1 accelerates growth and is often present during sporadic breast cancer progression. *Nature genetics*, *9*(4), 444–450. https://doi.org/10.1038/ng0495-444

Zámborszky, J., Szikriszt, B., Gervai, J. Z., Pipek, O., Póti, Á., Krzystanek, M., Ribli, D., Szalai-Gindl, J. M., Csabai, I., Szallasi, Z., Swanton, C., Richardson, A. L., & Szüts, D. (2017). Loss of BRCA1 or BRCA2 markedly increases the rate of base substitution mutagenesis and has distinct effects on genomic deletions. *Oncogene*, *36*(6), 746–755. https://doi.org/10.1038/onc.2016.243

Zhang, J., Chen, L., Zhang, J., & Wang, Y. (2019). Drug Inducible CRISPR/Cas Systems. *Computational and structural biotechnology journal*, *17*, 1171–1177. https://doi.org/10.1016/j.csbj.2019.07.015